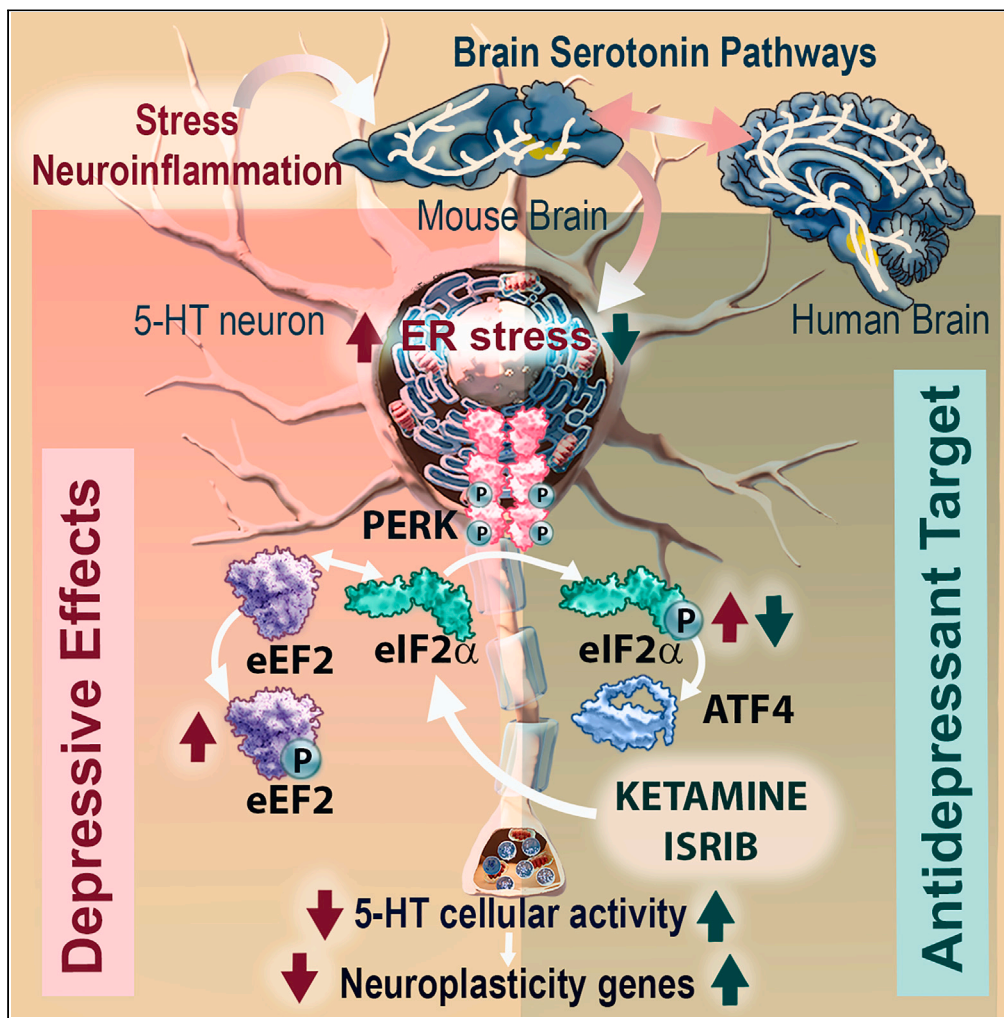


Article

ER stress in mouse serotonin neurons triggers a depressive phenotype alleviated by ketamine targeting eIF2 α signaling



Lluís Miquel-Rio, Unai Sarriés-Serrano, María Sancho-Alonso, ..., Leticia Campa, Fuencisla Pilar-Cuéllar, Analia Bortolozzi

lluís.miquel@iibb.csic.es (L.M.-R.)
analia.bortolozzi@iibb.csic.es (A.B.)

Highlights

ER stress on raphe 5-HT neurons triggers a depressive-like phenotype in mice

Altered eIF2 α pathway in 5-HT neurons induces global changes in brain neuroplasticity

EIF2 α signaling is critical in eliciting the rapid antidepressant effects of ketamine

Miquel-Rio et al., iScience 27, 109787
May 17, 2024 © 2024 The Authors. Published by Elsevier Inc.
<https://doi.org/10.1016/j.isci.2024.109787>



Article

ER stress in mouse serotonin neurons triggers a depressive phenotype alleviated by ketamine targeting eIF2 α signaling

Lluis Miquel-Rio,^{1,2,3,4,*} Unai Sarriés-Serrano,^{1,2,3,5} María Sancho-Alonso,^{1,2,3} Eva Florensa-Zanuy,^{3,6} Verónica Paz,^{1,2,3} Esther Ruiz-Bronchal,^{1,2,3} Sharon Manashirov,^{1,3,7} Leticia Campa,^{1,2,3} Fuencisla Pilar-Cuéllar,^{3,6} and Analia Bortolozzi^{1,2,3,8,*}

SUMMARY

Depression is a devastating mood disorder that causes significant disability worldwide. Current knowledge of its pathophysiology remains modest and clear biological markers are lacking. Emerging evidence from human and animal models reveals persistent alterations in endoplasmic reticulum (ER) homeostasis, suggesting that ER stress-related signaling pathways may be targets for prevention and treatment. However, the neurobiological basis linking the pathways involved in depression-related ER stress remains unknown. Here, we report that an induced model of ER stress in mouse serotonin (5-HT) neurons is associated with reduced *Egr1*-dependent 5-HT cellular activity and 5-HT neurotransmission, resulting in neuroplasticity deficits in forebrain regions and a depressive-like phenotype. Ketamine administration engages downstream eIF2 α signaling to trigger rapid neuroplasticity events that rescue the depressive-like effects. Collectively, these data identify ER stress in 5-HT neurons as a cellular pathway involved in the pathophysiology of depression and show that eIF2 α is critical in eliciting ketamine's fast antidepressant effects.

INTRODUCTION

Major depressive disorder (MDD) is a critical challenge to global mental health and the leading cause of mental health-related disability worldwide.¹ MDD is a highly prevalent mood disorder that negatively affects education, relationships, and employment and is prospectively associated with obesity, cardiovascular disease, and early death, including suicide.^{2,3} This disorder involved depressed mood, energy changes, sleep disorder, poor concentration, and lack of interest or excitement.^{4,5} Neuroimaging studies have identified structural and functional brain changes including volume reductions in cortical and subcortical structures,^{6,7} enlarged lateral ventricles, and white matter microstructural differences suggestive of compromised myelin integrity.^{8,9} In addition, histopathological studies have shown changes in neuron and glia density,^{10–12} and reduced the expression of synaptic proteins.^{13,14} In the same way, the number of synapses in the medial prefrontal cortex (mPFC) and hippocampus (HPC) is relatively low in patients with MDD and in rodent models.^{15,16} Hence, all converge that synaptic plasticity is key in the pathogenesis of MDD, although the pathophysiological mechanisms remain largely unknown.

Multiple evidences suggest that cellular stress contributes to the pathogenesis of complex diseases, such as cancer, diabetes and metabolic disorders, neurodegeneration, as well as cognitive and neuropsychiatric disorders.^{17–19} Indeed, it has been hypothesized that cellular stress linked to psychosocial stressors may be a major culprit to the progression of MDD.^{19–23} Within eukaryotic cells, the major organelle that shows an adaptive response to cellular stress is the endoplasmic reticulum (ER). Under normal conditions, the ER regulates multiple biological processes, such as the protein synthesis, folding, maturation, and transport, maintaining protein homeostasis for proper cellular functions.^{24–26} Moreover, the ER is responsible for calcium storage and the biosynthesis of lipids and sterols.²⁵ However, under stress signals, ER dysregulation results in the accumulation of unfolded/misfolded proteins in the ER lumen known as ER stress (ERS). To counteract this damaging effect and prevent apoptosis, the unfolded protein response (UPR) pathway is activated.^{27,28} The UPR pathway is regulated by an essential ER chaperone, 78-kDa glucose-regulated protein (GRP78, also referred to as BiP), 94-kDa glucose-regulated protein (GRP94),

¹Institute of Biomedical Research of Barcelona (IBB), Spanish National Research Council (CSIC), 08036 Barcelona, Spain

²Systems Neuropharmacology Research Group, August Pi i Sunyer Biomedical Research Institute (IDIBAPS), 08036 Barcelona, Spain

³Biomedical Research Networking Center for Mental Health (CIBERSAM), Institute of Health Carlos III (ISCIII), 28029 Madrid, Spain

⁴University of Barcelona (UB), 08036 Barcelona, Spain

⁵University of the Basque Country UPV/EHU, E-48940 Leioa, Bizkaia, Spain

⁶Department of Molecular and Cellular Signaling, Institute of Biomedicine and Biotechnology of Cantabria (IBBTEC), University of Cantabria-CSIC, 39011 Santander, Spain

⁷miCure Therapeutics LTD., Tel-Aviv 6423902, Israel

⁸Lead contact

*Correspondence: lluis.miquel@iibb.csic.es (L.M.-R.), analia.bortolozzi@iibb.csic.es (A.B.)

<https://doi.org/10.1016/j.isci.2024.109787>



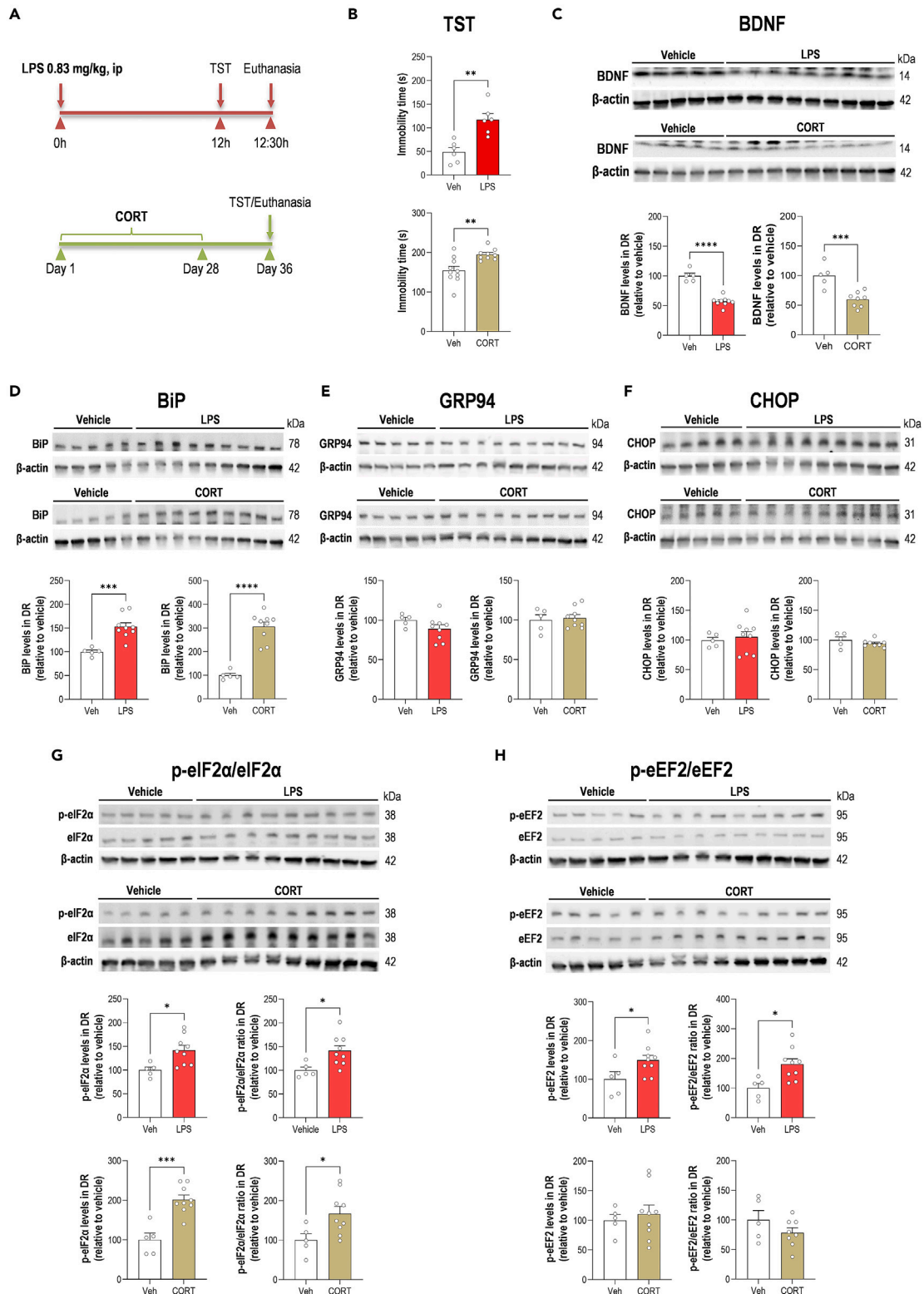


Figure 1. Activation of ERS in DR in mouse models based on lipopolysaccharide (LPS)-induced neuroinflammation or chronic exposure to corticosterone stress (CORT)

(A) Treatment schedule. Different groups of mice were treated with i) a single dose of LPS (0.83 mg/kg, ip) and examined 12 h post-administration, or ii) chronic CORT exposure in the drinking water for 28 days and examined on day 36.

(B) In the tail suspension test (TST), the immobility time was compared between Veh ($n = 6$) and LPS ($n = 6$) or Veh ($n = 10$) and CORT ($n = 9$) mice.

(C) BDNF protein levels in the DR were analyzed by Western blot (WB) and compared between Veh ($n = 5$) and LPS ($n = 9$) or Veh ($n = 5$) and CORT ($n = 8$) mice.

(D) BiP protein levels in the DR were analyzed by WB and compared between Veh ($n = 5$) and LPS ($n = 9$) or Veh ($n = 5$) and CORT ($n = 9$) mice.

(E) GRP94 protein levels in the DR were analyzed by WB and compared between Veh ($n = 5$) and LPS ($n = 9$) or Veh ($n = 5$) and CORT ($n = 9$) mice.

(F) CHOP protein levels in the DR were analyzed by WB and compared between Veh ($n = 5$) and LPS ($n = 9$) or Veh ($n = 5$) and CORT ($n = 8$) mice.

(G) eIF2 α and p-eIF2 α protein levels in the DR were analyzed by WB and compared between Veh ($n = 5$) and LPS ($n = 9$) or Veh ($n = 5$) and CORT ($n = 9$) mice.

(H) eEF2 and p-eEF2 protein levels in the DR were analyzed by WB and compared between Veh ($n = 5$) and LPS ($n = 9$) or Veh ($n = 5$) and CORT ($n = 9$) mice. Data are expressed as mean \pm SEM. * $p < 0.05$, ** $p < 0.01$, *** $p < 0.001$ by two-tailed t-test, see [File S1](#).

and three major signaling pathways: ER kinase-eukaryotic initiation factor 2 α (PERK-eIF2 α), activating transcription factor 6 (ATF6), and inositol-requiring enzyme 1 (IRE1), to alleviate cellular stress.²⁹ Among them, PERK-eIF2 α signaling is a particularly attractive target in synaptic plasticity processes, as well as being the main UPR pathway activated in neuroinflammation events linked to neurodegenerative and neuropsychiatric disorders.^{30–35} PERK is a highly conserved protein kinase that phosphorylates eIF2 α at the Ser51 site. Fine-tuning eIF2 α phosphorylation levels is pivotal in controlling eIF2 α -dependent protein synthesis, which underlies different learning and memory processes.³⁶ Indeed, PERK activation impairs learning function through the inactivation of cAMP response element-binding protein (CREB) signaling,³¹ while PERK inhibition improves cognitive function in animal models.³⁷ Furthermore, blockade of the phosphorylation-controlled translation of eIF2 α prevented long-term depression (LTD) and the internalization of AMPA receptors at hippocampal CA1 synapses.³⁸ Similarly, proper PERK-eIF2 α signaling in dopaminergic neurons is required for normal cognitive and motor functions.³⁹

Here, we explored the mechanisms by which PERK-eIF2 α signaling in raphe serotonin (5-HT) neurons, in the context of ERS, contribute to depressive phenotype. To this aim, we induced mouse models that developed ERS in the raphe nuclei. Our results establish raphe eIF2 α phosphorylation as a key mediator of 5-HT-dependent neuroplasticity processes and strongly support it as a site of the antidepressant action of ketamine.

RESULTS

Involvement of the endoplasmic reticulum stress in the dorsal raphe nucleus in depressive-like mouse models

We first verified whether PERK-eIF2 α signaling in raphe nuclei is linked to depressive phenotype using two well-established depressive-like male mouse models based on lipopolysaccharide (LPS)-induced neuroinflammation or chronic exposure to corticosterone stress (CORT)^{40,41} (Figure 1A). Both mouse models showed a depressive-like phenotype characterized by increased immobility time in the tail suspension test (TST) and reduced levels of brain-derived neurotrophic factor (BDNF) in the dorsal raphe nucleus (DR), a trophic marker strongly implicated in the pathophysiology of MDD,^{42,43} compared to vehicle-treated mice (Figures 1B and 1C). In addition, BiP protein levels, but not GRP94 nor CHOP, were statistically significantly increased to $153 \pm 4\%$ and $305 \pm 20\%$ in the DR of LPS- or CORT-treated mice, respectively, compared to their control groups (Figures 1D–1F). Upregulation of BiP protein activated downstream PERK-eIF2 α signaling, and we detected statistically significant increases in phosphorylated eIF2 α (p-eIF2 α) protein levels and p-eIF2 α /eIF2 α ratio in both depressive-like mouse models (Figure 1G). Since a cross-talk between eIF2 α and eukaryotic elongation factor 2 (eEF2) pathways has been reported,⁴⁴ phosphorylation was also evaluated in eEF2, resulting in statistically significant increases in the p-eEF2/eEF2 in DR in the LPS model, but not in CORT model, compared to the control group (Figure 1H). Taken together, these findings point to ERS and abnormal PERK-eIF2 α signaling in the DR are involved in the depressive-like behaviors, as previously described in the HPC and mPFC in mouse models of stress.⁴⁵

Tunicamycin-induced endoplasmic reticulum stress in raphe 5-HT neurons leads to a depressive phenotype

To confirm if ERS in raphe 5-HT neurons is involved in depressive-like behavior, we adopted an acute ERS model using a single infusion of tunicamycin (Tm, N-glycosylation inhibitor, 200 η g/ μ L) in DR and different groups of male mice were examined at 1, 3, and 7-day later (Figure 2A), as previously reported.⁴⁶ Control group received 1 μ L of vehicle (4% dimethyl sulfoxide - DMSO in artificial cerebrospinal fluid - aCSF). Other control groups of mice received locally 1 μ L of aCSF or DMSO (4% in aCSF) in DR, and no observable behavioral changes such as drinking, eating, or differences in TST immobility time or neuronal survival assessed using NeuN marker were detected in both experimental groups (Figure S1), as previously reported.^{47–49} Tm-treated mice showed an increased immobility time in the TST at 1 and 3 days after infusion (Figure 2B), and evoked anxious-like behavior in the dark-light box (DLB, 3 days later) compared to vehicle-treated mice (Figure 2C). None of these behaviors were associated with abnormal locomotor activity in the open field test (OFT) (Figure 2D). However, the behavioral profile changed 7 days later. Tm-treated male mice showed performances in TST and DLB comparable to those of vehicle-treated mice 7 days later; instead, they exhibited hypermobility in the OFT followed by a catatonic-like state and some of them died (Figures 2B–2D). Indeed, Tm induced a statistically significant increase in apoptotic CHOP protein levels in the DR only 7 days later, reaching $1422 \pm 221\%$ compared to the control group (Figure S2A). Next, we focused on the studies using the Tm-induced ERS model at 1 and 3 days later, in which the same treatment did not change the levels of CHOP protein, as well as NeuN, Iba1, and GFAP proteins (Figures S2A–S2D).

Up-regulated levels of BiP and GRP94 proteins were detected in the DR of Tm-treated mice, resulting in the phosphorylation of eIF2 α protein and increases in the p-eIF2 α /eIF2 α ratio 1- and 3-day after Tm infusion (Figures 2E–2G). Phosphorylation was also

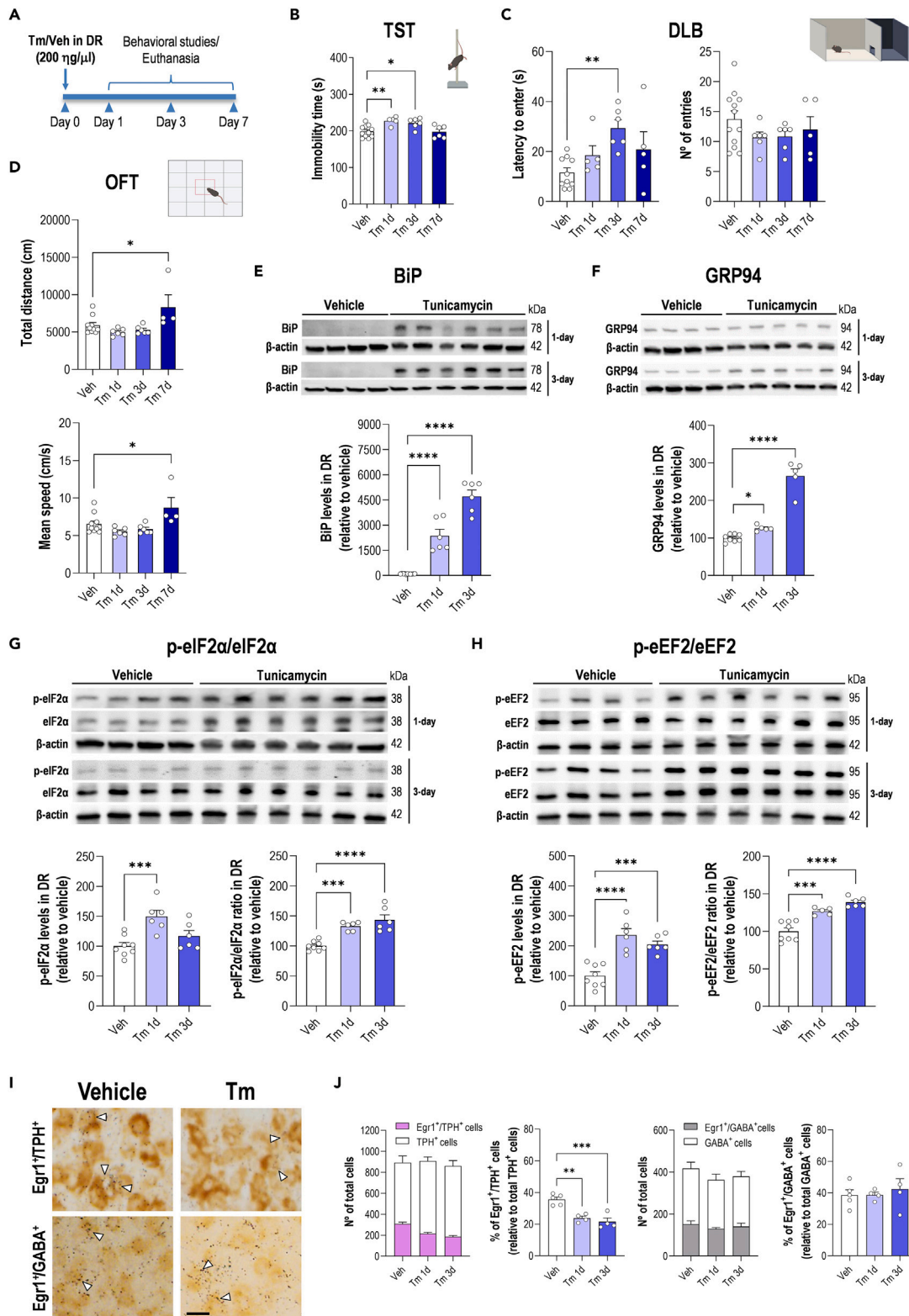


Figure 2. Activating ERS in DR induces a depressive-like phenotype in mice

(A) Schematic time course diagram. Mice were injected with 1 μ l tunicamycin (Tm, 200 $\text{ng}/\mu\text{l}$) or vehicle (Veh, 4% DMSO in artificial cerebrospinal fluid-aCSF) into the dorsal raphe nucleus (DR) and examined after 1, 3, and 7 days.

Figure 2. Continued

- (B) In the tail suspension test (TST), the immobility time of Veh ($n = 11$) and Tm ($n = 6$) mice was compared.
- (C) In the dark-light box (DLB), latency to enter and the number of entries into the light chamber were compared between Veh ($n = 11$) and Tm ($n = 6$) mice.
- (D) During the 15 min observation period, the total distance and mean speed were recorded for Veh ($n = 10$) and Tm ($n = 6$) mice in the open field test (OFT).
- (E) BiP protein levels in the DR were analyzed by Western blot (WB) and compared between Veh ($n = 11$) and Tm ($n = 6$) mice.
- (F) GRP94 protein levels in the DR were analyzed by WB and compared between Veh ($n = 8$) and Tm ($n = 5$) mice.
- (G) eIF2 α and p-eIF2 α protein levels in the DR were analyzed by WB and compared between Veh ($n = 8$) and Tm ($n = 6$) mice.
- (H) eEF2 and p-eEF2 protein levels in the DR were analyzed by WB and compared between Veh ($n = 8$) and Tm ($n = 6$) mice.
- (I) Photomicrographs showing TPH-positive or GABA-positive cells expressing Egr1 mRNA (^{33}P -oligonucleotide silver grains) in the DR of Veh and Tm mice. Scale bar: 20 μm . White arrowheads indicate TPH-positive or GABA-positive cells co-localizing with Egr1 mRNA.
- (J) The total number of TPH-positive or GABA-positive cells and the percentage of TPH- or GABA-positive cells expressing Egr1 mRNA were analyzed in Veh ($n = 5$) and Tm ($n = 4$) mice. Data are expressed as mean \pm SEM. * $p < 0.05$, ** $p < 0.01$, *** $p < 0.001$, **** $p < 0.0001$ by one-way ANOVA, see [File S3](#). See also [Figures S1–S3](#).

detected in eEF2, resulting in a statistically significant increase in the p-eEF2/eEF2 ratio at 1- and 3-day ([Figure 2H](#)). To further investigate the effects of ERS in the DR, we assessed the cellular response of 5-HT and GABA neurons using the early growth response 1 (Egr1) marker after Tm treatment. These results showed that ERS in DR significantly reduced the response of 5-HT neurons assessed as a lower number of cells co-localizing Egr1 and the 5-HT marker tryptophan hydroxylase-TPH at 1 and 3 days after Tm infusion (double Egr1/TPH-positive cells: vehicle, $35 \pm 2\%$; Tm 1-day, $24 \pm 1\%$; Tm 3-day, $21 \pm 2\%$) ([Figures 2I](#) and [2J](#)). However, the number of cells co-localizing positive for Egr1 and GABA was not modified (double Egr1/GABA-positive cells: vehicle, $38 \pm 4\%$; Tm-1 day, $39 \pm 2\%$; Tm-3 days, $42 \pm 6\%$). No changes in the total number of TPH- or GABA-positive cells were observed after a single intra-DR Tm infusion ([Figure 2J](#)). Collectively, these findings indicate that Tm-induced ERS model in DR leads to depressive/anxious-like behavioral abnormalities dependent on serotonergic cellular activity.

Although we initially focused our research on the ERS in male mice, in an additional experiment, the intra-DR application of Tm (200 ng/ μL , 1 μL) also induced increased immobility time in the TST in female mice compared to the control group ([Figure S3A](#)). In parallel, Tm-treated females showed up-regulated BiP and GRP94 protein levels in DR compared to vehicle-treated female mice ([Figure S3B](#)). Notably, changes in BiP levels did not lead to downstream changes in eIF2 α and p-eIF2 α protein levels ([Figure S3C](#)), as observed in Tm-treated males, suggesting that sex-associated factors may influence the cellular response to ERS in raphe 5-HT neurons.^{50,51}

Endoplasmic reticulum stress in raphe 5-HT neurons triggers reduced 5-HT neurotransmission and neuroplasticity gene expression in efferent brain regions

Functional deficits in monoamine neurotransmission, particularly 5-HT, have been widely associated with anxiety and depression.^{52,53} Next, we performed microdialysis experiments in the mPFC, which is strongly innervated by DR 5-HT neurons,^{54,55} to examine whether local ERS translates into changes in forebrain 5-HT neurotransmission ([Figure 3A](#)). These experiments were performed using only the 1-day Tm model. No differences in baseline extracellular 5-HT concentration were found in mPFC between the different groups (vehicle: 8.7 ± 1.3 , Tm 1-day: 8.6 ± 0.8 expressed as fmol/20 min fraction). Infusion of the depolarizing agent veratridine (50 μM) by reverse dialysis increased extracellular 5-HT levels in the mPFC of both group of mice, being this effect significantly greater in vehicle-treated mice ($p < 0.05$), suggesting deficits in intracellular 5-HT stores in Tm-treated mice ([Figure 3B](#)). Furthermore, the systemic administration of 5-HT $_{1A}$ receptor agonist 8-OH-DPAT (1 mg/kg, intraperitoneal – ip) comparably reduced 5-HT release in the mPFC of both groups of mice. Following systemic 8-OH-DPAT administration, extracellular 5-HT levels returned to baseline values in vehicle-treated mice 1 h later, as previously reported,⁵⁶ but remained reduced in Tm-treated mice ($p < 0.05$) ([Figure 3C](#)). Therefore, local ERS blunted the activity of raphe 5-HT neurons and mice showed reduced forebrain 5-HT release and an altered adaptive response of the inhibitory feedback mechanism mediated by the presynaptic activation of the 5-HT $_{1A}$ receptor.

Neurotrophic growth factors (e.g., BDNF) and angiogenesis-endothelial signaling factors are required for activity-dependent synapse formation and maintenance.⁴³ As previously mentioned, reduced levels of BDNF have been reported in patients with MDD and in depressive-like animal models.^{16,42,43,57,58} Notably, BDNF levels are increased following the use of conventional (e.g., selective inhibitors of 5-HT transporter – SSRI) and fast-acting (e.g., ketamine, non-competitive glutamate N-methyl-D-aspartate receptor –NMDAR– antagonist) antidepressants.⁵⁹ Both SSRIs and ketamine directly promote signaling and occupancy of the TrkB receptor by BDNF.⁶⁰ We therefore investigated whether local ERS stimulation in raphe 5-HT neurons induces changes in the transcription of neuroplasticity genes in 5-HT efferent neural circuits ([Figures 3D](#), [S4](#), and [S5](#)). We found that intra-DR Tm application 1-day later significantly reduced BDNF mRNA levels in 5-HT projection brain areas including mPFC, cingulate cortex (Cg), HPC subfields, amygdala (Amg), and habenular nuclei (Hb) ([Figure 3E](#)). Similarly, TrkB receptor mRNA levels decreased in several HPC subfields, while neurtin and vascular endothelial growth factor (VEGF) expression was markedly reduced in all brain areas analyzed in Tm-treated mice compared to vehicle-treated mice ([Figures 3F](#), [3G](#), and [3I](#)). The mRNA levels of postsynaptic density protein 95 (PSD95), a critical downstream mediator of BDNF-induced plasticity, were also downregulated in HPC, Amg, and Hb in intra-DR Tm-treated mice ([Figure 3H](#)). Moreover, Tm-induced ERS in DR statistically significantly reduced Egr1 mRNA expression throughout the brain ([Figure 3J](#)). These results uncover that a focal change in DR 5-HT cellular activity under the ERS and attenuation of 5-HT neurotransmission translate into a global change in brain neuroplasticity/function, possibly by virtue of divergent 5-HT projections that target many distinct brain regions.⁶¹

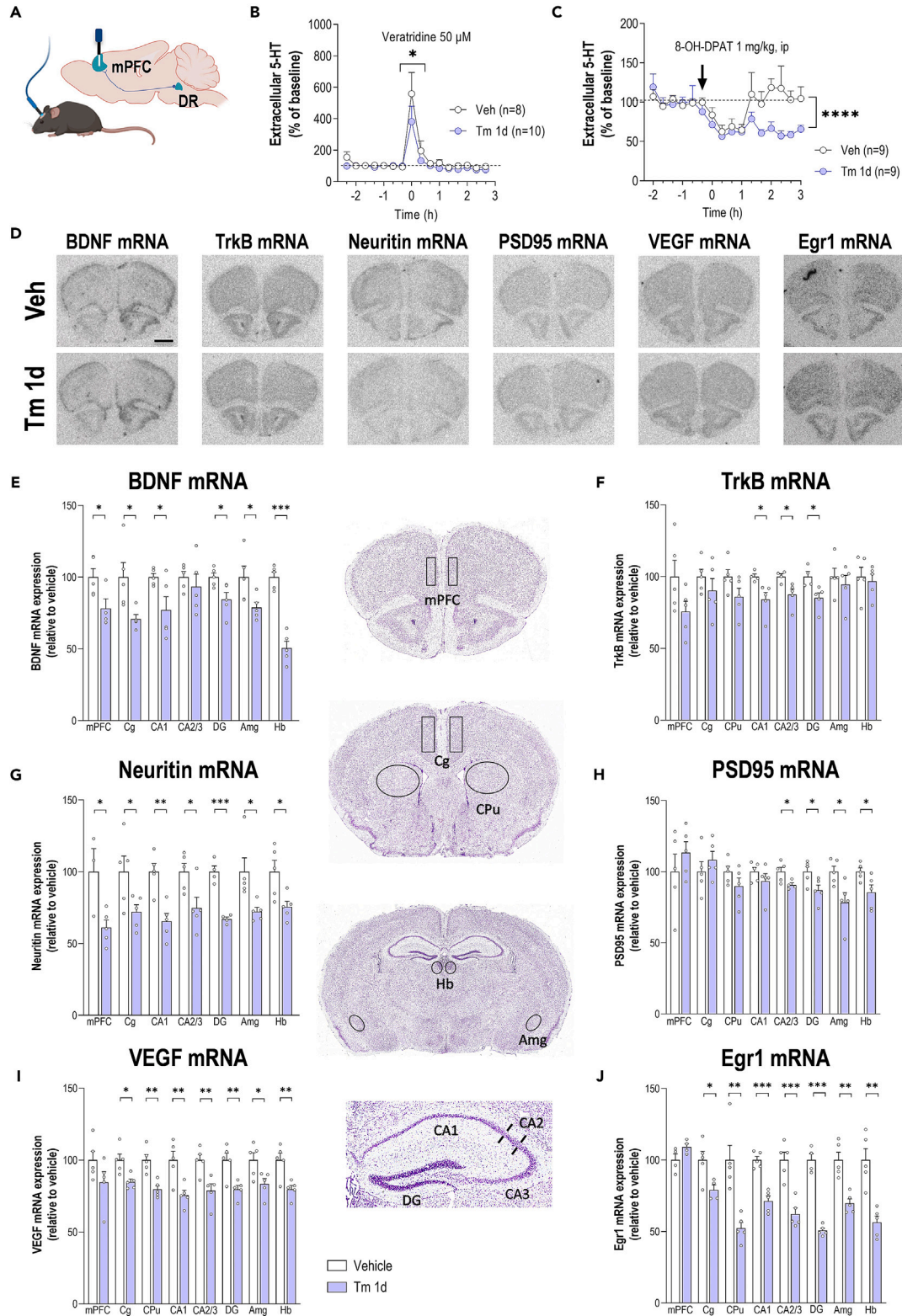


Figure 3. ERS in 5-HT neurons is associated with reduced 5-HT neurotransmission and transcriptional changes in plasticity genes in the forebrain
(A) Schematic representation of an *in vivo* microdialysis procedure to measure 5-HT release. Mice injected with 1 μ L Tm (200 η g/ μ L) or Veh (aCSF+DMSO 4%) into the DR were implanted with a dialysis probe in the medial prefrontal cortex (mPFC). Microdialysis experiments were performed 24 h later.

Figure 3. Continued

(B) The local effect of veratridine (depolarizing agent, 50 μ M) on 5-HT release in the mPFC was examined in Veh ($n = 8$) and Tm ($n = 10$) mice.

(C) The effect of the systemic administration of 8-OH-DPAT (selective 5-HT_{1A} receptor agonist, 1 mg/kg, ip) on prefrontal 5-HT release was analyzed in Veh ($n = 9$) and Tm ($n = 9$) mice.

(D) Representative images of coronal sections of mouse mPFC showing mRNA expression of BDNF, TrkB, Neurtin, PSD95, VEGF, and Egr1 in Veh and Tm mice assessed by *in situ* hybridization. Scale bar: 1 mm.

(E–J) The relative density of BDNF, TrkB, Neurtin, PSD95, VEGF, and Egr1 mRNA expression in the different brain areas was compared between Veh and Tm mice ($n = 5$ /group). Coronal sections of mouse brain stained with cresyl-violet show quantification ROIs in mPFC, cingulate cortex (Cg), caudate-putamen (CPU), subfields of the hippocampus (CA1, CA2, CA3, and dentate gyrus - DG), amygdala (Amg), and habenular nuclei (Hb). Data are expressed as mean \pm SEM. * $p < 0.05$, ** $p < 0.01$, *** $p < 0.001$ by two-way ANOVA (B and C) or one-way ANOVA (E–J), see [File S6](#). See also [Figures S4](#) and [S5](#).

Ketamine mitigates local endoplasmic reticulum stress in raphe 5-HT neurons and ameliorates the depressive phenotype

The impact of ERS on raphe 5-HT neurons underlying the depressive phenotype was further investigated in the Tm-treated mouse model using the fast-acting antidepressant (*R,S*)-ketamine (referred to as ketamine - Ket). Mice received intra-DR Tm or vehicle and 24 h later were injected (ip) with an effective dose of ketamine as antidepressant (10 mg/kg) or saline.^{12,62} These mice were tested 30 min or 48 h later (corresponding to Tm 1-day and 3-day groups, respectively) in the TST to assess the antidepressant-like response to ketamine ([Figure 4A](#)). We found that the Tm-induced behavioral depressive phenotype was rescued by ketamine 30 min later ($p < 0.0001$), and mice showed a decrease in the immobility time on TST suggestive of an antidepressant response ([Figure 4B](#)). In contrast, the effect of ketamine was no longer observed 48 h after administration, as previously reported also with (*S*)-ketamine,⁶³ and Tm+Ket-treated mice exhibited an increased immobility response in the TST similar to that of Tm+Veh-treated mice ([Figure 4B](#)). We also examined the effect of ketamine on BDNF protein levels in DR after local ERS, since BDNF signaling is essential for its antidepressant action.^{64,65} Indeed, Ket-treated mice (10 mg/kg, ip) showed statistically significantly increased BDNF protein levels in the DR 30 min and 48 h later (Ket 30 min: $162 \pm 7\%$; Ket 48 h: $127 \pm 5\%$ relative to vehicle) ([Figure S6A](#)). More important, a single ketamine dose (10 mg/kg, ip) was able to reverse the reduction of BDNF levels induced by ERS in the DR (1-day, Tm+Veh: $53 \pm 6\%$, Tm+Ket: $86 \pm 10\%$; 3-day, Tm+Veh: $69 \pm 4\%$, Tm+Ket: $135 \pm 10\%$ relative to vehicle) ([Figure 4C](#)). Although these effects may involve a ketamine-induced blockade of NMDAR typically activated by glutamate neurotransmission outside the DR,^{64,66} a direct ketamine effect on 5-HT neurons may also occur, since different NMDAR subunits were co-localized with the 5-HT marker TPH ([Figures 4D](#) and [S7](#)).

Next, we assessed whether ketamine inhibits the activation of the ERS and PERK-eIF2 α signaling pathways in DR. Since acute ketamine treatment (10 mg/kg, ip) did not affect BiP levels in DR compared to vehicle-treated mice (Ket 30 min: $111 \pm 8\%$; Ket 48 h: $112 \pm 11\%$ relative to vehicle), this group of mice was not systematically tested in the next assays ([Figure S6B](#)). The Tm-induced increase in BiP and GRP94 protein levels in DR was reversed by ketamine 30 min after injection ($p < 0.05$) ([Figures 4E](#) and [4F](#)). Although, surprisingly, we found that 48 h after ketamine administration, BiP and GRP94 levels in DR were comparable or even higher than those of the Tm+Veh group ($p < 0.05$) ([Figures 4E](#) and [4F](#)). In parallel, Tm-treated mice showed a statistically significant decrease in *p*-eIF2 α levels and improved *p*-eIF2 α /eIF2 α ratio after ketamine application, observed at both 30 min and 48 h later ([Figures 4G](#) and [S6C](#)). Ketamine treatment also partially enhanced eEF2 signaling by reducing *p*-eEF2 in the DR after local ERS ([Figure 4H](#)). Taken together, these data support that the administration of ketamine attenuated local ERS, restored downstream eIF2 α signaling pathway, and increased BDNF levels in the DR. Normalization of these events in 5-HT neurons may contribute to the amelioration of the Tm-induced depressive phenotype.

Targeting eIF2 α signaling in dorsal raphe nucleus drives ketamine antidepressant responses

As reported, ketamine exerts its rapid antidepressant action by eliciting eEF2-dependent homeostatic synaptic scaling,^{64,67} as well as through cell-specific translation via eukaryotic initiation factor 4E (eIF4E).⁶⁸ In addition, eIF2 α -dependent translation is a key molecular process underlying synaptic plasticity.^{36,37,69,70} Therefore, we further explored whether the disruption of PERK-eIF2 α signaling pathway, and eventually eEF2, prevents the antidepressant action of ketamine in the Tm-induced ERS mouse model in DR. We used the small molecule ISRIB (integrated stress response inhibitor), which blocks downstream *p*-eIF2 α signaling under ERS or salubrinal (SAL), an eIF2 α dephosphorylation inhibitor (eIF2 α -GADD34:PP1 phosphatase inhibitor)^{71–73} ([Figure 5A](#)). While treatment with ISRIB (0.25 mg/kg, ip, two doses) facilitated ketamine-induced reversal of BiP levels in DR after local ERS, SAL (1 mg/kg, ip, two doses) prevented the effect of ketamine, and mice treated with Tm+SAL+Ket showed a marked increase in BiP protein levels compared to Tm+Ket-treated mice ([Figure 5B](#)). It is important to note that ISRIB treatment slightly blocked the induction of BiP levels in DR in response to ERS ($p = 0.06$), whereas SAL increased them ([Figure S8A](#)). However, both ISRIB and SAL increased DR GRP94 protein levels and inhibited the marginal effect of ketamine on GRP94 ($p = 0.08$) in the Tm mouse model ([Figures 5B](#) and [S8A](#)). We then confirmed that blockade of eIF2 α dephosphorylation by SAL prevented the effect of ketamine and detected increases in *p*-eIF2 α , *p*-eEF2, and their ratios in the DR of mice treated with Tm+SAL+Ket compared to Tm+Ket-treated mice ([Figures 5C](#) and [5D](#)). Similarly, SAL treatment induced statistically significant increases in *p*-eIF2 α /eIF2 α and *p*-eEF2/eEF2 ratios in DR mice 1 day after Tm infusion ([Figures S8B](#) and [S8C](#)). In contrast, ISRIB treatment facilitated ketamine-induced eIF2 α and eEF2 signaling in the ERS mouse model, and the *p*-eIF2 α /eIF2 α and *p*-eEF2/eEF2 ratios were similarly reduced in the Tm+Ket and Tm+ISRIB+Ket groups ([Figures 5C](#) and [5D](#)). Notably, treatment with ISRIB alone decreased Tm-induced eEF2 phosphorylation ([Figure S8C](#)), consistent with previous reports showing that ISRIB modifies basal *p*-eEF2 levels in several cell lines.⁷⁴

Next, we assessed the behavioral depressive phenotype after ERS in raphe 5-HT neurons and found that ISRIB treatment potentiates the acute antidepressant effect of ketamine, but SAL prevents antidepressant ketamine actions ([Figure 5E](#)). Moreover, ISRIB significantly enhanced ketamine-induced BDNF level in DR of Tm mice, while SAL treatment displayed the opposite effect by decreasing the BDNF level

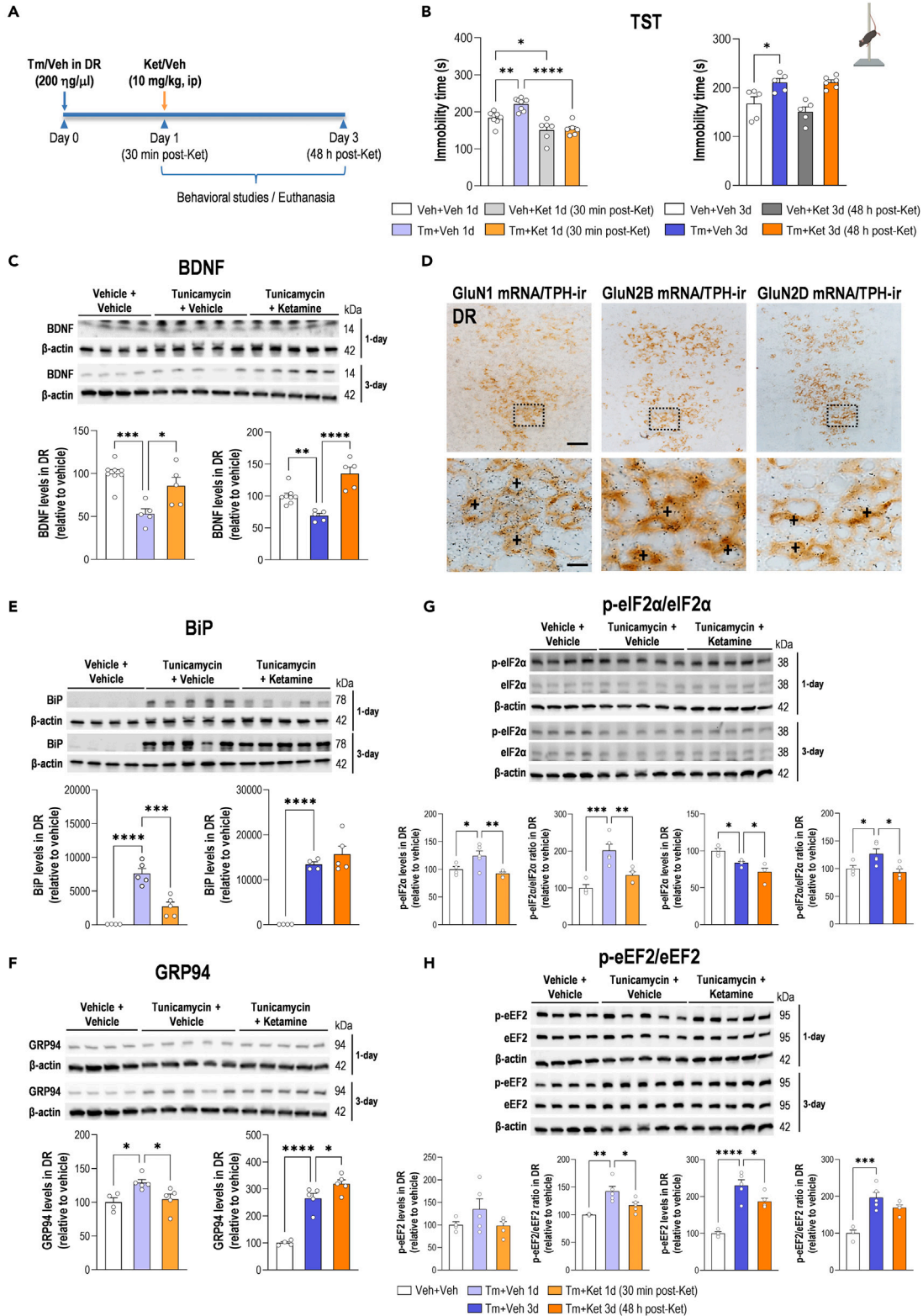


Figure 4. Continued

- (B) In the TST, the immobility time was recorded in Ket-treated Veh and Tm mice ($n = 5$ to 8 per group).
- (C) BDNF protein levels in the DR were analyzed by WB. They were compared between Veh and Tm mice treated with Ket ($n = 5$ to 8 per group).
- (D) Representative coronal midbrain sections showing TPH-positive cells expressing different NMDAR subunits including GluN1, GluN2B, and GluN2D mRNA in the DR of wild-type mice. The bottom row shows high magnification photomicrographs of the frames in the top row. The + symbol indicates TPH- and NMDA subunits-positive cells. Scale bars: low = $100\ \mu\text{m}$, high = $20\ \mu\text{m}$.
- (E) BiP protein levels in the DR were analyzed by WB and compared between Veh and Tm mice treated with Ket ($n = 4$ to 5 per group).
- (F) GRP94 protein levels in the DR were analyzed by WB and compared between Ket-treated Veh and Tm mice ($n = 4$ to 5 per group).
- (G) eIF2 α and p-eIF2 α protein levels in the DR were analyzed by WB and compared between Ket-treated Veh and Tm mice ($n = 4$ to 5 per group).
- (H) eEF2 and p-eEF2 protein levels in the DR were analyzed by WB and compared between Ket-treated Veh and Tm mice ($n = 4$ to 5 per group). Data are expressed as mean \pm SEM. * $p < 0.05$, ** $p < 0.01$, *** $p < 0.001$, **** $p < 0.0001$ by one-way ANOVA, see [File S7](#). See also [Figures S6](#) and [S7](#).

([Figure 5F](#)). Importantly, ISRIB alone also reduced immobility time in the TST in Tm-treated mice, but did not change BDNF levels, suggesting a behavioral antidepressant response ([Figures S8D](#) and [S8E](#)).

Raphe 5-HT neurons project to and modulate multiple highly interconnected cortical and sub-cortical brain circuitry. As noted above, the impairment of 5-HT neurotransmission is implicated in MDD.^{52,53} Our observation that the depressive-like phenotype in raphe ERS mice was reversed with ISRIB (or ketamine+ISRIB) led us to hypothesize that the role of the PERK-eIF2 α pathway in 5-HT neurons function may be critical for the proper modulation of target area neuroplasticity. Hence, we systematically analyzed the transcription of neuroplasticity and cell activation genes in the different 5-HT projection brain areas after pharmacological treatment with ISRIB or SAL and ketamine using the mouse model of local ERS in the DR ([Figures 5G](#) and [S9–S12](#)). We found that the sustained induction of p-eIF2 α in DR by SAL showed slight effects on neuroplasticity gene transcription in the different brain areas analyzed, e.g., reduced TrkB mRNA expression only in Cg and CPu in Tm+SAL mice ([Figures S13](#) and [S14](#)). However, SAL treatment significantly worsened the effects of ketamine on BDNF, TrkB, and VEGF mRNA levels in the mPFC in the ERS model ([Figures 5G](#) and [S9](#)). A similar pattern was observed in almost all 5-HT projection brain areas analyzed, where SAL prevented the effect of ketamine on synaptic plasticity ([Figures S9–S12](#)). In contrast, ISRIB-induced blockade of p-eIF2 α effects under ERS conditions in DR increased the transcription of some neuroplasticity genes such as BDNF, neuritin, and VEGF in all brain areas analyzed ([Figures S13](#) and [S14](#)). Furthermore, ISRIB also enhanced the effect of ketamine on the expression of TrkB and PSD95 in cortical and subcortical brain areas, among others ([Figures 5G](#) and [S9–S12](#)). Taken together, these data are consistent with the idea that the disruption of PERK-eIF2 α signaling under ERS in raphe 5-HT neurons may contribute to the depressive phenotype. Ketamine reversed the effects of Tm on ERS in the DR and the depressive phenotype, but this did not occur under conditions of selective eIF2 α -GADD34:PP1 blockade, suggesting that the eIF2 α signaling pathway plays a key role in the antidepressant mechanism of action of ketamine, particularly under ERS.

DISCUSSION

In recent years, several clinical and preclinical studies have shown a strong connection between neuropsychiatric disorders, including MDD, and ERS and PERK-dependent downstream UPR pathway.^{19–23,75–77} Activation of PERK signaling via eIF2 α phosphorylation is thought to alter neuronal function by repressing global protein synthesis, particularly the synthesis and expression of a cluster of proteins crucial for the establishment of synapses and neuronal plasticity.⁷⁸ This type of PERK-eIF2 α -dependent translation might account not only for synaptic failure, but also for subsequent mood, emotion, and cognitive decline observed in neuropsychiatric disorders.^{2,3,16} Here we report that local ERS and altered PERK-eIF2 α signaling in raphe 5-HT neurons 1) induced a despair-like behavior in mice, 2) reduced the expression of the cell activity marker Egr1 selectively in 5-HT neurons, 3) impaired 5-HT neurotransmission in the forebrain, and 4) decreased the transcription of several MDD-related trophic growth factors and angiogenesis-endothelial signaling factors in 5-HT-innervated brain areas. Treatment with the fast-acting ketamine antidepressant alleviated despair symptoms and restored synaptic plasticity by normalizing PERK-eIF2 α signaling regionally in the DR. Notably, upregulated ERS and PERK-eIF2 α pathway markers have also been detected in DR in two well-established mouse models of depressive-like behavior. Therefore, understanding the role that ERS plays in a specific cellular system, such as the 5-HT system, and the response to treatment holds considerable potential for the successful therapeutic management of depressive disorders.

The brain 5-HT system exerts its widespread effects from a group of relatively small brainstem nuclei known as the raphe nuclei. Among them, DR—one of the most extensively connected hubs in the mammalian brain—is the largest serotonergic nucleus, containing approximately one-third of all 5-HT neurons in the brain.^{79,80} Efferent DR 5-HT fibers collectively innervate and connect most functionally distinct brain areas and changes in the activity of DR 5-HT neurons have been implicated with several human disorders (or disease models thereof) with broad symptomatology, such as MDD, autism, and neurodegenerative diseases.^{81,82} In the present study, we hypothesized that the regional induction of ERS and aberrant PERK-eIF2 α downstream signaling in the DR is sufficient to drive a depressive-like phenotype. Using a pharmacological paradigm, we demonstrated that Tm-dependent ERS activation reduces the cellular 5-HT activity, but not GABAergic activity, in the DR. New evidence using single-cell RNA sequencing (scRNA-seq) showed that DR contain not only clusters of 5-HT neurons (TPH-positive cells), but also GABAergic and glutamatergic neurons that do not express TPH and hence do not release 5-HT.⁸³ Clusters of peptidergic and dopaminergic neurons, which show molecular and functional heterogeneity, have also identified in DR.^{83,84} However, a systematic analysis of the anatomical organization of these non-5-HT DR projections is still lacking. Some pioneering anterograde tracing studies demonstrated that the extended amygdala receives abundant inputs from DR non-5-HT neurons, although the specific neuronal type has not been confirmed.^{85,86} On the contrary, systematic mapping studies using state-of-the-art techniques (combining scRNA-seq, *in situ* hybridization, and anatomical tracing) revealed that 5-HT neurons within the DR innervate the entire forebrain and midbrain with well-defined

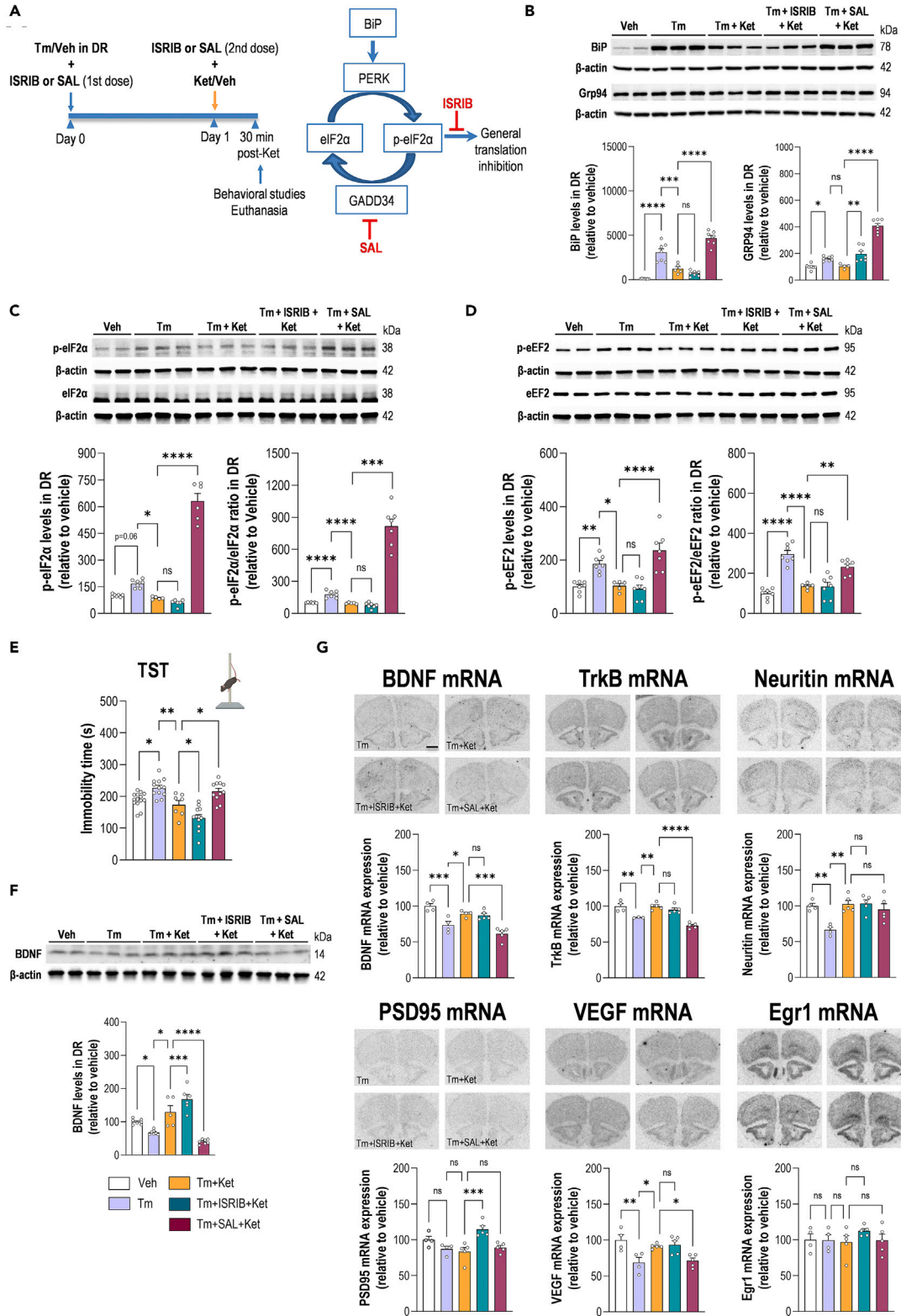


Figure 5. eIF2 α signaling in 5-HT neurons is critical to the antidepressant effects of ketamine

(A) Treatment schedule. Mice were injected with 1 μ L Tm (200 ng/ μ L) or Veh (aCSF+DMSO 4%) into the DR and received two doses of ISRIB (PERK inhibitor, 0.25 mg/kg, ip) or Salubrinal (SAL, eIF2 α -GADD34:PP1 phosphatase inhibitor, 1 mg/kg, ip). Ket (10 mg/kg, ip) was administered 24 h later and mice were examined 30 min after Ket administration.

(B) BiP and GRP94 protein levels in mouse DR were analyzed by WB and the effects of ISRIB or SAL on Ket action were compared ($n = 7$ per group).

(C) eIF2 α and p-eIF2 α protein levels in mouse DR were analyzed by WB and the effects of ISRIB or SAL on Ket action were compared ($n = 7$ per group).

(D) eEF2 and p-eEF2 protein levels in mouse DR were analyzed by WB and the effects of ISRIB or SAL on Ket action were compared ($n = 7$ per group).

(E) In the TST, the immobility time was recorded in mice ($n = 7$ to 14 per group).

(F) BDNF protein levels in DR were analyzed by WB. They were compared between Veh and Tm mice treated with ISRIB or SAL and Ket ($n = 5$ to 7 per group).

(G) Representative images of coronal sections of the mPFC showing the mRNA expression of BDNF, TrkB, Neurtin, PSD95, VEGF, and Egr1 in the mouse model of Tm assessed by *in situ* hybridization. Scale bar: 1 mm. The relative density of mRNA expression of the different transcripts was compared between Veh and Tm mice treated with ISRIB or SAL and Ket ($n = 4$ to 5 per group). Data are expressed as mean \pm SEM. * $p < 0.05$, ** $p < 0.01$, *** $p < 0.001$, **** $p < 0.0001$ by one-way ANOVA, see [File S9](#). See also [Figures S8–S14](#).

anatomical projection patterns.^{80–82} This anatomical organization is consistent with our data showing that reduced 5-HT function, decreased cell 5-HT activity and neurotransmission under local ERS is associated with downregulated levels of neuroplasticity gene expression throughout the brain, e.g., BDNF, neurtin, and VEGF. The importance of BDNF and other synaptic markers examined in this study is that they are intertwined with other depression-related molecular pathways. Notably, BDNF is a downstream target of the 5-HT signaling cascade, which is further supported by other studies.^{16,87} Thus, it is tempting to speculate that local ERS activation in DR 5-HT neurons results in a depressive phenotype by impacting brain-wide synaptic plasticity by the virtue of the anatomical expansion of the 5-HT system, although the precise mechanisms by which 5-HT neurons propagate this signal remain unknown. It is important to note that present results were found in male mice, but some sex-specific differences have been described at the level of transcriptomic clusters in DR 5-HT neurons.⁸⁴ Therefore, an exhaustively comparative analysis between male and female mice will provide evidence of sex differences linked to ERS activation in 5-HT neurons and depressive phenotype.⁸⁸

Recent studies indicated that intra-hippocampal Tm injection is an effective way to induce ERS that elicits behavioral deficits suggestive of a depressive-like state in rats.^{35,89} This was correlated with the increased expression of UPR genes, namely *Grp94*, *Grp78*, *Xbp-1*, *Atf6*, *Atf4*, and *Chop*, as well as several genes relevant to inflammation reinforcing the idea that UPR signaling acts in a pro-inflammatory environment, as described in postmortem brain samples from subjects with MDD.⁹⁰ In addition, decreased expression of synaptic plasticity genes such as BDNF, PSD95, and synaptophysin in the HPC has also been described in this rat model with Tm, but the proposed mechanism associated with UPR activation is unknown.³⁵ Our results support that decreased levels in neuroplasticity gene expression could be dependent on the activation of PERK-eIF2 α signaling, as observed in DR after Tm application. In this sense, the inhibition of eIF2 α dephosphorylation by SAL increased the negative effects of Tm on the synaptic markers (e.g., BDNF and TrkB) in some of the brain areas analyzed. More importantly, treatment with ISRIB, which restores the downstream translation of eIF2 α , blocked the local Tm-induced ERS in DR, increasing the levels of synaptic markers and resulting in an improvement of the depressive phenotype. Further, ISRIB was reported to improve cognitive functions in rodents by diminishing ATF4 and CHOP expression.⁹¹ Compounds as these may help alleviate some of the cognitive and emotional impairment associated with depression, as well as mitigate the physiological responses resulting from ERS and UPR activation.

Altered functional connectivity of neural circuits caused by abnormal synaptic plasticity is thought to be central to the response to negative emotions.^{42,43} The fast-acting antidepressant ketamine triggers a form of homeostatic synaptic plasticity dependent on NMDAR blockade and also BDNF pathway.^{67,92} The most widely accepted view is that ketamine-mediated NMDAR blockade, in turn, stops eEF2 kinase activity, leading to a gradual loss of eEF2 phosphorylation and de-suppression of BDNF translation, ultimately triggering TrkB receptor signaling. TrkB signaling and subsequent rapid homeostatic synaptic plasticity are required to elicit not only rapid effects of ketamine, but also its sustained effects.⁹² Further work showed that eIF4E is also a key effector in ketamine-induced hippocampal synaptic plasticity and that the 4E-BPs-eIF4E partner is necessary for the antidepressant effect of ketamine (e.g., hypophosphorylated 4E-BPs bind to eIF4E preventing protein synthesis).⁶⁸ Our data support that the integrity of the PERK-eIF2 α pathway is also required for ketamine' antidepressant action. Although the precise mechanism by which ketamine reduces eIF2 α phosphorylation in DR is unknown, we hypothesize that ketamine either inhibits the activity and/or expression of one of the eIF2 α kinases or stimulates the activity of eIF2 α phosphatases to reduce p-eIF2 α levels in DR. Pharmacological inhibition of eIF2 α phosphorylation effects with ISRIB enhanced the antidepressant behavioral response to ketamine. In contrast, the sustained upregulation of p-eIF2 α in the DR of the Tm mouse model blocked ketamine-induced antidepressant behavior and neuroplasticity in 5-HT efferent brain regions. These effects likely converge on 5-HT neurons, as PERK-eIF2 α activation was induced locally in the DR, and ketamine-target NMDAR was found to co-localize with the selective 5-HT neuron marker TPH. Supporting these data, NMDA applied locally into the DR acts directly on 5-HT neurons, inducing excitatory responses.⁹³

In summary, we show here that pathophysiological situations associated with ERS in DR 5-HT neurons induced a depressive-like phenotype in mice. We provide evidence that impaired PERK-eIF2 α signaling in 5-HT neurons is a critical mediator underlying the global changes in brain neuroplasticity that give rise to the altered behavioral phenotype. The current findings also show that eIF2 α signaling in 5-HT neurons is essential for the antidepressant actions of ketamine. Blockade of eIF2 α de-phosphorylation inhibits the effect of ketamine, while the inhibition of downstream p-eIF2 α effects by ISRIB potentiates it. Taken together, these data provide a further insight into the cellular mechanisms linking ERS to the pathophysiology of MDD and provide a solid basis for future studies focusing on eIF2 α as a potential new antidepressant target.

Limitations of the study

Our current study has some limitations. Here, we focus on the ERS in 5-HT neurons and its role in depression using predominantly male mice in the different animal models. However, it is important to note that sex hormones and sexual dimorphism may influence the cellular response to ERS in different tissues/cells.^{50,51} Furthermore, some sex differences in 5-HT neurons in DR have been described at the transcriptomic level.⁸⁴ In line with this, we have recently reported sex-dependent changes in the PERK-eIF2 α signaling pathway in 5-HT neurons and a sex-specific antidepressant response in a mouse model of misfolded protein accumulation and ERS.⁸⁸ Finally, in the pilot experiment we conducted here, we showed that Tm-induced ERS also resulted in a depressive phenotype in female mice, but did not modify the p-eIF2 α /eIF2 α ratio. Therefore, research targeting sex differences may contribute to a better understanding of ERS in depression and lead directly to the development of sex-specific therapeutic interventions.

In addition, Tm is a well-known pharmacological strategy to induce local ERS and aberrant downstream signaling in different brain areas.^{35,46} In the ERS model in DR herein, the local application of Tm increased ERS markers (e.g., BiP, GRP94), leaving an activation of the PERK-eIF2 α pathway, and contributing to the development of a depressive phenotype. However, Tm does not selectively disrupt the PERK-eIF2 α pathway, and other components of the UPR pathway may be affected. Further experiments investigating the cell type-specific modulation of PERK-eIF2 α signaling in 5-HT neurons may identify the physiological role of PERK in 5-HT neuronal function involved in emotional functioning and cognitive processes, and provide insight into how the dysregulation of PERK-eIF2 α signaling may be involved in neuropsychiatric disorders. Therefore, studies aimed at addressing the rate and extent of eIF2 α phosphorylation and its close relationship with the eEF2 pathway in 5-HT neurons would be relevant. In support of this, recent progress has been made in elucidating the role of the selective disruption of the PERK-eIF2 α pathway in DA neurons on motor and cognitive function.³⁹

STAR★METHODS

Detailed methods are provided in the online version of this paper and include the following:

- **KEY RESOURCES TABLE**
- **RESOURCE AVAILABILITY**
 - Lead contact
 - Materials availability
 - Data and code availability
- **EXPERIMENTAL MODEL AND STUDY PARTICIPANT DETAILS**
 - Animals
 - LPS mouse model
 - CORT mouse model
 - Tunicamycin mouse model
- **METHOD DETAILS**
 - Groups and drug treatments
 - Behavioral analysis
 - Open field test (OFT)
 - Light and dark box test (DLB)
 - Tail suspension test (TST)
 - *In situ* hybridization (ISH)
 - Western Blot (WB)
 - *In vivo* microdialysis
- **QUANTIFICATION AND STATISTICAL ANALYSIS**

SUPPLEMENTAL INFORMATION

Supplemental information can be found online at <https://doi.org/10.1016/j.isci.2024.109787>.

ACKNOWLEDGMENTS

This work was supported by MCIU/AEI/FEDER, UE grant (PID2019-105136RB-100, MCIN/AEI/10.13039/501100011033 to AB, and SAF2015-67457-R to FPC), Fundación La Marató TV3 (202207), and AGAUR 2021-SGR-01358, Catalan Government. CB/07/09/0034 and CB/07/09/0008 Center for Networked Biomedical Research on Mental Health (CIBERSAM). We also thank the Spanish Stress Research Network, MCIN/AEI/10.13039/501100011033. USS is a recipient of a fellowship from the Non-Doctor Researcher Formation Pre-doctoral Program of Basque Government, Spain. MSA has a Margarita Salas Grant (MS21-132) from the University of Valencia (requalification of the Spanish University System of the Ministry of Universities of the Government of Spain, financed by the European Union, Next Generation EU).

AUTHOR CONTRIBUTIONS

Conceptualization and supervision of the research: A.B. Methodology: L.M.R, U.S.S, and M.S.A performed stereotaxic surgeries and ran behavioral and WB experiments; E.R.B, E.F.Z, S.M, and F.P.C ran behavioral experiments in CORT and LPS models; V.P performed *in situ* hybridization and immunohistochemistry; L.C. performed 5-HT analysis using HPLC. L.M.R analyzed and supervised the data. Writing: AB with all nine authors' inputs. Funding acquisition: A.B. All authors edited and approved the final version of the article.

DECLARATION OF INTERESTS

The authors declare no competing interests.

Received: October 27, 2023

Revised: February 19, 2024

Accepted: April 16, 2024

Published: April 18, 2024

REFERENCES

- Herrman, H., Kieling, C., McGorry, P., Horton, R., Sargent, J., and Patel, V. (2019). Reducing the global burden of depression: a Lancet-World Psychiatric Association Commission. *Lancet* 393, e42–e43. [https://doi.org/10.1016/S0140-6736\(18\)32408-5](https://doi.org/10.1016/S0140-6736(18)32408-5).
- Malhi, G.S., and Mann, J.J. (2018). Depression. *Lancet* 392, 2299–2312. [https://doi.org/10.1016/S0140-6736\(18\)31948-2](https://doi.org/10.1016/S0140-6736(18)31948-2).
- Marwaha, S., Palmer, E., Suppes, T., Cons, E., Young, A.H., and Upthegrove, R. (2023). Novel and emerging treatments for major depression. *Lancet* 401, 141–153. [https://doi.org/10.1016/S0140-6736\(22\)02080-3](https://doi.org/10.1016/S0140-6736(22)02080-3).
- Otte, C., Gold, S.M., Penninx, B.W., Pariante, C.M., Etkin, A., Fava, M., Mohr, D.C., and Schatzberg, A.F. (2016). Major depressive disorder. *Nat. Rev. Dis. Primers* 2, 16065. <https://doi.org/10.1038/nrdp.2016.65>.
- Alexopoulos, G.S. (2019). Mechanisms and treatment of late-life depression. *Transl. Psychiatry* 9, 188. <https://doi.org/10.1038/s41398-019-0514-6>.
- Zhuo, C., Li, G., Lin, X., Jiang, D., Xu, Y., Tian, H., Wang, W., and Song, X. (2019). The rise and fall of MRI studies in major depressive disorder. *Transl. Psychiatry* 9, 335. <https://doi.org/10.1038/s41398-019-0680-6>.
- Nolan, M., Roman, E., Nasa, A., Levins, K.J., O'Hanlon, E., O'Keane, V., and William Roddy, D. (2020). Hippocampal and Amygdalar Volume Changes in Major Depressive Disorder: A Targeted Review and Focus on Stress. *Chronic Stress (Thousand Oaks)* 4, 2470547020944553. <https://doi.org/10.1177/2470547020944553>.
- Hellewell, S.C., Welton, T., Maller, J.J., Lyon, M., Korgaonkar, M.S., Koslow, S.H., Williams, L.M., Rush, A.J., Gordon, E., and Grieve, S.M. (2019). Profound and reproducible patterns of reduced regional gray matter characterize major depressive disorder. *Transl. Psychiatry* 9, 176. <https://doi.org/10.1038/s41398-019-0512-8>.
- Schmaal, L., Pozzi, E., C Ho, T., van Velzen, L.S., Veer, I.M., Opel, N., Van Someren, E.J.W., Han, L.K.M., Aftanas, L., Aleman, A., et al. (2020). ENIGMA MDD: seven years of global neuroimaging studies of major depression through worldwide data sharing. *Transl. Psychiatry* 10, 172. <https://doi.org/10.1038/s41398-020-0842-6>.
- Sanacora, G., and Banasr, M. (2013). From pathophysiology to novel antidepressant drugs: glial contributions to the pathology and treatment of mood disorders. *Biol. Psychiatry* 73, 1172–1179. <https://doi.org/10.1016/j.biopsych.2013.03.032>.
- Rajkowska, G., and Stockmeier, C.A. (2013). Astrocyte pathology in major depressive disorder: insights from human post-mortem brain tissue. *Curr. Drug Targets* 14, 1225–1236. <https://doi.org/10.2174/13894501113149990156>.
- Fullana, M.N., Ruiz-Bronchal, E., Ferrés-Coy, A., Juárez-Escoto, E., Artigas, F., and Bortolozzi, A. (2019). Regionally selective knockdown of astroglial glutamate transporters in infralimbic cortex induces a depressive phenotype in mice. *Glia* 67, 1122–1137. <https://doi.org/10.1002/glia.23593>.
- Duric, V., Banasr, M., Stockmeier, C.A., Simen, A.A., Newton, S.S., Overholser, J.C., Jurjus, G.J., Dieter, L., and Duman, R.S. (2013). Altered expression of synapse and glutamate related genes in post-mortem hippocampus of depressed subjects. *Int. J. Neuropsychopharmacol.* 16, 69–82. <https://doi.org/10.1017/S1461145712000016>.
- Li, J., Seidlitz, J., Suckling, J., Fan, F., Ji, G.J., Meng, Y., Yang, S., Wang, K., Qiu, J., Chen, H., and Liao, W. (2021). Cortical structural differences in major depressive disorder correlate with cell type-specific transcriptional signatures. *Nat. Commun.* 12, 1647. <https://doi.org/10.1038/s41467-021-21943-5>.
- Kang, H.J., Voleti, B., Hajszan, T., Rajkowska, G., Stockmeier, C.A., Licznarski, P., Lepack, A., Majik, M.S., Jeong, L.S., Banasr, M., et al. (2012). Decreased expression of synapse-related genes and loss of synapses in major depressive disorder. *Nat. Med.* 18, 1413–1417. <https://doi.org/10.1038/nm.2886>.
- Fries, G.R., Saldana, V.A., Finnstein, J., and Rein, T. (2023). Molecular pathways of major depressive disorder converge on the synapse. *Mol. Psychiatry* 28, 284–297. <https://doi.org/10.1038/s41380-022-01806-1>.
- Zhu, J., Xu, S., Gao, W., Feng, J., and Zhao, G. (2019). Honokiol induces endoplasmic reticulum stress-mediated apoptosis in human lung cancer cells. *Life Sci.* 221, 204–211. <https://doi.org/10.1016/j.lfs.2019.01.046>.
- Costa-Mattioli, M., and Walter, P. (2020). The integrated stress response: From mechanism to disease. *Science* 368, eaat5314. <https://doi.org/10.1126/science.aat5314>.
- Díaz-Hung, M.L., Martínez, G., and Hetz, C. (2020). Emerging roles of the unfolded protein response (UPR) in the nervous system: A link with adaptive behavior to environmental stress? *Int. Rev. Cell Mol. Biol.* 350, 29–61. <https://doi.org/10.1016/bs.ircmb.2020.01.004>.
- Bown, C., Wang, J.F., MacQueen, G., and Young, L.T. (2000). Increased temporal cortex ER stress proteins in depressed subjects who died by suicide. *Neuropsychopharmacology* 22, 327–332. [https://doi.org/10.1016/S0893-133X\(99\)00091-3](https://doi.org/10.1016/S0893-133X(99)00091-3).
- Nevell, L., Zhang, K., Aiello, A.E., Koenen, K., Galea, S., Soliven, R., Zhang, C., Wildman, D.E., and Uddin, M. (2014). Elevated systemic expression of ER stress related genes is associated with stress-related mental disorders in the Detroit Neighborhood Health Study. *Psychoneuroendocrinology* 43, 62–70. <https://doi.org/10.1016/j.psyneuen.2014.01.013>.
- Timberlake, M.A., and Dwivedi, Y. (2015). Altered Expression of Endoplasmic Reticulum Stress Associated Genes in Hippocampus of Learned Helpless Rats: Relevance to Depression Pathophysiology. *Front. Pharmacol.* 6, 319. <https://doi.org/10.3389/fphar.2015.00319>.
- Yoshino, Y., and Dwivedi, Y. (2020). Elevated expression of unfolded protein response genes in the prefrontal cortex of depressed subjects: Effect of suicide. *J. Affect. Disord.* 262, 229–236. <https://doi.org/10.1016/j.jad.2019.11.001>.
- Ellgaard, L., and Helenius, A. (2003). Quality control in the endoplasmic reticulum. *Nat. Rev. Mol. Cell Biol.* 4, 181–191. <https://doi.org/10.1038/nrm1052>.
- Burdakov, D., Petersen, O.H., and Verkhratsky, A. (2005). Intraluminal calcium as a primary regulator of endoplasmic reticulum function. *Cell Calcium* 38, 303–310. <https://doi.org/10.1016/j.ceca.2005.06.010>.
- McCaffrey, K., and Braakman, I. (2016). Protein quality control at the endoplasmic reticulum. *Essays Biochem.* 60, 227–235. <https://doi.org/10.1042/EBC20160003>.
- Hetz, C., and Papa, F.R. (2018). The unfolded protein response and cell fate control. *Mol. Cell* 69, 169–181. <https://doi.org/10.1016/j.molcel.2017.06.017>.
- Hetz, C., Zhang, K., and Kaufman, R.J. (2020). Mechanisms, regulation and functions of the unfolded protein response. *Nat. Rev. Mol. Cell Biol.* 21, 421–438. <https://doi.org/10.1038/s41580-020-0250-z>.
- Gardner, B.M., Pincus, D., Gotthardt, K., Gallagher, C.M., and Walter, P. (2013). Endoplasmic reticulum stress sensing in the unfolded protein response. *Cold Spring*

- Harb. *Perspect. Biol.* 5, a013169. <https://doi.org/10.1101/cshperspect.a013169>.
30. Ma, T., Trinh, M.A., Wexler, A.J., Bourbon, C., Gatti, E., Pierre, P., Cavener, D.R., and Klann, E. (2013). Suppression of eIF2 α kinases alleviates Alzheimer's disease-related plasticity and memory deficits. *Nat. Neurosci.* 16, 1299–1305. <https://doi.org/10.1038/nn.3486>.
 31. Sen, T., Gupta, R., Kaiser, H., and Sen, N. (2017). Activation of PERK Elicits Memory Impairment through Inactivation of CREB and Downregulation of PSD95 After Traumatic Brain Injury. *J. Neurosci.* 37, 5900–5911. <https://doi.org/10.1523/JNEUROSCI.2343-16.2017>.
 32. Tang, J., Yu, W., Chen, S., Gao, Z., and Xiao, B. (2018). Microglia Polarization and Endoplasmic Reticulum Stress in Chronic Social Defeat Stress Induced Depression Mouse. *Neurochem. Res.* 43, 985–994. <https://doi.org/10.1007/s11064-018-2504-0>.
 33. Li, M.X., Li, Q., Sun, X.J., Luo, C., Li, Y., Wang, Y.N., Chen, J., Gong, C.Z., Li, Y.J., Shi, L.P., et al. (2019). Increased Homer1-mGluR5 mediates chronic stress-induced depressive-like behaviors and glutamatergic dysregulation via activation of PERK-eIF2 α . *Prog. Neuro-Psychopharmacol. Biol. Psychiatry* 95, 109682. <https://doi.org/10.1016/j.pnpb.2019.109682>.
 34. Xu, X.F., Shi, M.M., Luo, M.Y., Liu, D.D., Guo, D.M., Ling, C., Zhong, X.L., Xu, Y., and Cao, W.Y. (2022). Targeting PERK mediated endoplasmic reticulum stress attenuates neuroinflammation and alleviates lipopolysaccharide-induced depressive-like behavior in male mice. *Int. Immunopharmacol.* 111, 109092. <https://doi.org/10.1016/j.intimp.2022.109092>.
 35. Yuan, G., Xiao, L., Xie, Y., Si, L., Xu, H., Xu, W., and Wang, G. (2023). Tunicamycin induces depression-like behaviors in male rats, accompanied by initiated chaperon-mediated autophagy and decreased synaptic protein expression in the hippocampus. *Neurosci. Lett.* 798, 137058. <https://doi.org/10.1016/j.neulet.2023.137058>.
 36. Sharma, V., Sood, R., Khlaifia, A., Eslamizade, M.J., Hung, T.Y., Lou, D., Asgarifafshajani, A., Lalzar, M., Kiniry, S.J., Stokes, M.P., et al. (2020). eIF2 α controls memory consolidation via excitatory and somatostatin neurons. *Nature* 586, 412–416. <https://doi.org/10.1038/s41586-020-2805-8>.
 37. Sharma, V., Ounallah-Saad, H., Chakraborty, D., Hleihil, M., Sood, R., Barrera, I., Edry, E., Kolatt Chandran, S., Ben Tabou de Leon, S., Kaphzan, H., and Rosenblum, K. (2018). Local Inhibition of PERK Enhances Memory and Reverses Age-Related Deterioration of Cognitive and Neuronal Properties. *J. Neurosci.* 38, 648–658. <https://doi.org/10.1523/JNEUROSCI.0628-17.2017>.
 38. Di, P.G.V., Huang, W., Buffington, S.A., Hsu, C.C., Bonnen, P.E., Placzek, A.N., Sidrauski, C., Krnjević, K., Kaufman, R.J., Walter, P., and Costa-Mattioli, M. (2014). Translational control of mGluR-dependent long-term depression and object-place learning by eIF2 α . *Nat. Neurosci.* 17, 1073–1082. <https://doi.org/10.1038/nn.3754>.
 39. Longo, F., Mancini, M., Ibraheem, P.L., Aryal, S., Mesini, C., Patel, J.C., Penhos, E., Rahman, N., Mamcarz, M., Santini, E., et al. (2021). Cell-type-specific disruption of PERK-eIF2 α signaling in dopaminergic neurons alters motor and cognitive function. *Mol. Psychiatry* 26, 6427–6450. <https://doi.org/10.1038/s41380-021-01099-w>.
 40. Ferrés-Coy, A., Galofré, M., Pilar-Cuellar, F., Vidal, R., Paz, V., Ruiz-Bronchal, E., Campa, L., Pazos, Á., Caso, J.R., Leza, J.C., et al. (2016). Therapeutic antidepressant potential of a conjugated siRNA silencing the serotonin transporter after intranasal administration. *Mol. Psychiatry* 21, 328–338. <https://doi.org/10.1038/mp.2015.80>.
 41. Florensa-Zanuy, E., Garro-Martínez, E., Adell, A., Castro, E., Díaz, Á., Pazos, Á., Mac-Dowell, K.S., Martín-Hernández, D., and Pilar-Cuellar, F. (2021). Cannabidiol antidepressant-like effect in the lipopolysaccharide model in mice: Modulation of inflammatory pathways. *Biochem. Pharmacol.* 185, 114433. <https://doi.org/10.1016/j.bcp.2021.114433>.
 42. Duman, R.S., and Monteggia, L.M. (2006). A neurotrophic model for stress-related mood disorders. *Biol. Psychiatry* 59, 1116–1127. <https://doi.org/10.1016/j.biopsych.2006.02.013>.
 43. Duman, R.S., Aghajanian, G.K., Sanacora, G., and Krystal, J.H. (2016). Synaptic plasticity and depression: new insights from stress and rapid-acting antidepressants. *Nat. Med.* 22, 238–249. <https://doi.org/10.1038/nm.4050>.
 44. Lin, Y., Yang, C.C., McQuary, P., Rosa Campos, A., Aza Blanc, P., and Wolf, D.A. (2019). Cross Talk between eIF2 α and eEF2 Phosphorylation Pathways Optimizes Translational Arrest in Response to Oxidative Stress. *iScience* 20, 466–480. <https://doi.org/10.1016/j.isci.2019.09.031>.
 45. Mao, J., Hu, Y., Ruan, L., Ji, Y., and Lou, Z. (2019). Role of endoplasmic reticulum stress in depression. *Mol. Med. Rep.* 20, 4774–4780. <https://doi.org/10.3892/mmr.2019.10789>.
 46. Cóppola-Segovia, V., Cavarsan, C., Maia, F.G., Ferraz, A.C., Nakao, L.S., Lima, M.M., and Zanata, S.M. (2017). ER Stress Induced by Tunicamycin Triggers α -Synuclein Oligomerization, Dopaminergic Neurons Death and Locomotor Impairment: a New Model of Parkinson's Disease. *Mol. Neurobiol.* 54, 5798–5806. <https://doi.org/10.1007/s12035-016-0114-x>.
 47. Kelava, T., Cavar, I., and Culo, F. (2010). Influence of small doses of various drug vehicles on acetaminophen-induced liver injury. *Can. J. Physiol. Pharmacol.* 88, 960–967. <https://doi.org/10.1139/y10-065>.
 48. Soltani, N., Mohammadi, E., Allahavakoli, M., Shamsizadeh, A., Roohbakhsh, A., and Haghparast, A. (2016). Effects of Dimethyl Sulfoxide on Neuronal Response Characteristics in Deep Layers of Rat Barrel Cortex. *Basic Clin. Neurosci.* 7, 213–220. <https://doi.org/10.15412/J.BCN.03070306>.
 49. Reimer, L., Haikal, C., Gram, H., Theologidis, V., Kovacs, G., Ruesink, H., Baun, A., Nielsen, J., Otzen, D.E., Li, J.Y., and Jensen, P.H. (2022). Low dose DMSO treatment induces oligomerization and accelerates aggregation of α -synuclein. *Sci. Rep.* 12, 3737. <https://doi.org/10.1038/s41598-022-07706-2>.
 50. Sari, F.R., Watanabe, K., Widyantoro, B., Thandavarayan, R.A., Harima, M., Kodama, M., and Aizawa, Y. (2011). Sex differences play a role in cardiac endoplasmic reticulum stress (ERS) and ERS-initiated apoptosis induced by pressure overload and thapsigargin. *Cardiovasc. Pathol.* 20, 281–290. <https://doi.org/10.1016/j.carpath.2010.07.006>.
 51. Zarate, S.M., Pandey, G., Chilukuri, S., Garcia, J.A., Cude, B., Storey, S., Salem, N.A., Bancroft, E.A., Hook, M., and Srinivasan, R. (2021). Cytisine is neuroprotective in female but not male 6-hydroxydopamine lesioned parkinsonian mice and acts in combination with 17- β -estradiol to inhibit apoptotic endoplasmic reticulum stress in dopaminergic neurons. *J. Neurochem.* 157, 710–726. <https://doi.org/10.1111/jnc.15282>.
 52. Berton, O., and Nestler, E.J. (2006). New approaches to antidepressant drug discovery: beyond monoamines. *Nat. Rev. Neurosci.* 7, 137–151. <https://doi.org/10.1038/nrn1846>.
 53. Krishnan, V., and Nestler, E.J. (2008). The molecular neurobiology of depression. *Nature* 455, 894–902. <https://doi.org/10.1038/nature07455>.
 54. Amargós-Bosch, M., Bortolozzi, A., Puig, M.V., Serrats, J., Adell, A., Celada, P., Toth, M., Mengod, G., and Artigas, F. (2004). Co-expression and in vivo interaction of serotonin1A and serotonin2A receptors in pyramidal neurons of prefrontal cortex. *Cereb. Cortex* 14, 281–299. <https://doi.org/10.1093/cercor/bhg128>.
 55. Santana, N., Bortolozzi, A., Serrats, J., Mengod, G., and Artigas, F. (2004). Expression of serotonin1A and serotonin2A receptors in pyramidal and GABAergic neurons of the rat prefrontal cortex. *Cereb. Cortex* 14, 1100–1109. <https://doi.org/10.1093/cercor/bbh070>.
 56. Bortolozzi, A., Amargós-Bosch, M., Toth, M., Artigas, F., and Adell, A. (2004). In vivo efflux of serotonin in the dorsal raphe nucleus of 5-HT1A receptor knockout mice. *J. Neurochem.* 88, 1373–1379. <https://doi.org/10.1046/j.1471-4159.2003.02267.x>.
 57. Bus, B.A.A., Molendijk, M.L., Tendolkar, I., Penninx, B.W.J.H., Prickaerts, J., Elzinga, B.M., and Voshaar, R.C.O. (2015). Chronic depression is associated with a pronounced decrease in serum brain-derived neurotrophic factor over time. *Mol. Psychiatry* 20, 602–608. <https://doi.org/10.1038/mp.2014.83>.
 58. Kishi, T., Yoshimura, R., Ikuta, T., and Iwata, N. (2017). Brain-Derived Neurotrophic Factor and Major Depressive Disorder: Evidence from Meta-Analyses. *Front. Psychiatry* 8, 308. <https://doi.org/10.3389/fpsy.2017.00308>.
 59. Castrén, E., and Monteggia, L.M. (2021). Brain-Derived Neurotrophic Factor Signaling in Depression and Antidepressant Action. *Biol. Psychiatry* 90, 128–136. <https://doi.org/10.1016/j.biopsych.2021.05.008>.
 60. Casarotto, P.C., Gyrych, M., Fred, S.M., Kovaleva, V., Moliner, R., Enkavi, G., Biojone, C., Cannarozzo, C., Sahu, M.P., Kaurinkoski, K., et al. (2021). Antidepressant drugs act by directly binding to TRKB neurotrophin receptors. *Cell* 184, 1299–1313.e19. <https://doi.org/10.1016/j.cell.2021.01.034>.
 61. Miquel-Rio, L., Sarriés-Serrano, U., Pavia-Collado, R., Meana, J.J., and Bortolozzi, A. (2023). The Role of α -Synuclein in the Regulation of Serotonin System: Physiological and Pathological Features. *Biomedicines* 11, 541. <https://doi.org/10.3390/biomedicines11020541>.
 62. Fullana, M.N., Paz, V., Artigas, F., and Bortolozzi, A. (2022). Ketamine triggers rapid antidepressant effects by modulating synaptic plasticity in a new depressive-like mouse model based on astrocyte glutamate transporter GLT-1 knockdown in infralimbic cortex. *Rev. Psiquiatr. Salud Ment. (Engl Ed)* 15, 94–100. <https://doi.org/10.1016/j.rpsmen.2022.06.008>.
 63. Fukumoto, K., Toki, H., Iijima, M., Hashihayata, T., Yamaguchi, J.I., Hashimoto, K., and Chaki, S. (2017). Antidepressant Potential of (R)-Ketamine in Rodent Models: Comparison with (S)-Ketamine. *J. Pharmacol.*

- Exp. Ther. 361, 9–16. <https://doi.org/10.1124/jpet.116.239228>.
64. Autry, A.E., Adachi, M., Nosyreva, E., Na, E.S., Los, M.F., Cheng, P.F., Kavalali, E.T., and Monteggia, L.M. (2011). NMDA receptor blockade at rest triggers rapid behavioural antidepressant responses. *Nature* 475, 91–95. <https://doi.org/10.1038/nature10130>.
 65. Lin, P.Y., Ma, Z.Z., Mahgoub, M., Kavalali, E.T., and Monteggia, L.M. (2021). A synaptic locus for TrkB signaling underlying ketamine rapid antidepressant action. *Cell Rep.* 36, 109513. <https://doi.org/10.1016/j.celrep.2021.109513>.
 66. Gideons, E.S., Kavalali, E.T., and Monteggia, L.M. (2014). Mechanisms underlying differential effectiveness of memantine and ketamine in rapid antidepressant responses. *Proc. Natl. Acad. Sci. USA* 111, 8649–8654. <https://doi.org/10.1073/pnas.1323920111>.
 67. Kavalali, E.T., and Monteggia, L.M. (2020). Targeting Homeostatic Synaptic Plasticity for Treatment of Mood Disorders. *Neuron* 106, 715–726. <https://doi.org/10.1016/j.neuron.2020.05.015>.
 68. Aguilar-Valles, A., De Gregorio, D., Matta-Camacho, E., Eslamizade, M.J., Khlaifia, A., Skaleka, A., Lopez-Canul, M., Torres-Berrio, A., Bermudez, S., Rurak, G.M., et al. (2021). Antidepressant actions of ketamine engage cell-specific translation via eIF4E. *Nature* 590, 315–319. <https://doi.org/10.1038/s41586-020-03047-0>.
 69. Costa-Mattioli, M., Gobert, D., Stern, E., Gamache, K., Colina, R., Cuello, C., Sossin, W., Kaufman, R., Pelletier, J., Rosenblum, K., et al. (2007). eIF2 α phosphorylation bidirectionally regulates the switch from short- to long-term synaptic plasticity and memory. *Cell* 129, 195–206. <https://doi.org/10.1016/j.cell.2007.01.050>.
 70. Trinh, M.A., Kaphzan, H., Wek, R.C., Pierre, P., Cavener, D.R., and Klann, E. (2012). Brain-specific disruption of the eIF2 α kinase PERK decreases ATF4 expression and impairs behavioral flexibility. *Cell Rep.* 1, 676–688. <https://doi.org/10.1016/j.celrep.2012.04.010>.
 71. Sidrauski, C., Acosta-Alvear, D., Khoutorsky, A., Vedantham, P., Hearn, B.R., Li, H., Gamache, K., Gallagher, C.M., Ang, K.K.H., Wilson, C., et al. (2013). Pharmacological brake-release of mRNA translation enhances cognitive memory. *Elife* 2, e00498. <https://doi.org/10.7554/eLife.00498>.
 72. Wek, R.C. (2018). Role of eIF2 α Kinases in Translational Control and Adaptation to Cellular Stress. *Cold Spring Harb. Perspect. Biol.* 10, a032870. <https://doi.org/10.1101/cshperspect.a032870>.
 73. Zadorozhnyi, P.V., Pokotylo, I.O., Kiselev, V.V., Okhtina, O.V., and Kharchenko, A.V. (2019). Molecular docking studies of salubrinol and its analogs as inhibitors of the GADD34:PP1 enzyme. *ADMET DMPK.* 7, 140–150. <https://doi.org/10.5599/admet.632>.
 74. Jin, X., Xie, J., Zabolocki, M., Wang, X., Jiang, T., Wang, D., Désaubry, L., Bardy, C., and Proud, C.G. (2020). The prohibitin-binding compound fluorizoline affects multiple components of the translational machinery and inhibits protein synthesis. *J. Biol. Chem.* 295, 9855–9867. <https://doi.org/10.1074/jbc.RA120.012979>.
 75. So, J., Warsh, J.J., and Li, P.P. (2007). Impaired endoplasmic reticulum stress response in B-lymphoblasts from patients with Bipolar-I disorder. *Biol. Psychiatry* 62, 141–147. <https://doi.org/10.1016/j.biopsych.2006.10.014>.
 76. Gold, P.W., Licinio, J., and Pavlatou, M.G. (2013). Pathological para-inflammation and endoplasmic reticulum stress in depression: potential translational targets through the CNS insulin, klotho and PPAR- γ systems. *Mol. Psychiatry* 18, 154–165. <https://doi.org/10.1038/mp.2012.167>.
 77. Kim, P., Scott, M.R., and Meador-Woodruff, J.H. (2021). Dysregulation of the unfolded protein response (UPR) in the dorsolateral prefrontal cortex in elderly patients with schizophrenia. *Mol. Psychiatry* 26, 1321–1331. <https://doi.org/10.1038/s41380-019-0537-7>.
 78. Moreno, J.A., Radford, H., Peretti, D., Steinert, J.R., Verity, N., Martin, M.G., Halliday, M., Morgan, J., Dinsdale, D., Ortori, C.A., et al. (2012). Sustained translational repression by eIF2 α -P mediates prion neurodegeneration. *Nature* 485, 507–511. <https://doi.org/10.1038/nature11058>.
 79. Okaty, B.W., Commons, K.G., and Dymecki, S.M. (2019). Embracing diversity in the 5-HT neuronal system. *Nat. Rev. Neurosci.* 20, 397–424. <https://doi.org/10.1038/s41583-019-0151-3>.
 80. Okaty, B.W., Sturrock, N., Escobedo Lozoya, Y., Chang, Y., Senft, R.A., Lyon, K.A., Alekseyenko, O.V., and Dymecki, S.M. (2020). A single-cell transcriptomic and anatomic atlas of mouse dorsal raphe Pet1 neurons. *Elife* 9, e55523. <https://doi.org/10.7554/eLife.55523>.
 81. Muzerelle, A., Scotto-Lomassese, S., Bernard, J.F., Soiza-Reilly, M., and Gaspar, P. (2016). Conditional anterograde tracing reveals distinct targeting of individual serotonin cell groups (B5-B9) to the forebrain and brainstem. *Brain Struct. Funct.* 221, 535–561. <https://doi.org/10.1007/s00429-014-0924-4>.
 82. Huang, K.W., Ochandarena, N.E., Philson, A.C., Hyun, M., Birnbaum, J.E., Cicconet, M., and Sabatini, B.L. (2019). Molecular and anatomical organization of the dorsal raphe nucleus. *Elife* 8, e46464. <https://doi.org/10.7554/eLife.46464>.
 83. Pollak Dorocic, I., Fürth, D., Xuan, Y., Johansson, Y., Pozzi, L., Silberberg, G., Carlén, M., and Meletis, K. (2014). A whole-brain atlas of inputs to serotonergic neurons of the dorsal and median raphe nuclei. *Neuron* 83, 663–678. <https://doi.org/10.1016/j.neuron.2014.07.002>.
 84. Ren, J., Isakova, A., Friedmann, D., Zeng, J., Grutzner, S.M., Pun, A., Zhao, G.Q., Kolluru, S.S., Wang, R., Lin, R., et al. (2019). Single-cell transcriptomes and whole-brain projections of serotonin neurons in the mouse dorsal and median raphe nuclei. *Elife* 8, e49424. <https://doi.org/10.7554/eLife.49424>.
 85. Aznar, S., Qian, Z.X., and Knudsen, G.M. (2004). Non-serotonergic dorsal and median raphe projection onto parvalbumin- and calbindin-containing neurons in hippocampus and septum. *Neuroscience* 124, 573–581. <https://doi.org/10.1016/j.neuroscience.2003.12.020>.
 86. Halberstadt, A.L., and Balaban, C.D. (2008). Selective anterograde tracing of nonserotonergic projections from dorsal raphe nucleus to the basal forebrain and extended amygdala. *J. Chem. Neuroanat.* 35, 317–325. <https://doi.org/10.1016/j.jchemneu.2008.02.006>.
 87. Duric, V., and Duman, R.S. (2013). Depression and treatment response: dynamic interplay of signaling pathways and altered neural processes. *Cell. Mol. Life Sci.* 70, 39–53. <https://doi.org/10.1007/s00018-012-1020-7>.
 88. Sarriés-Serrano, U., Miquel-Rio, L., Paz, V., Meana, J.J., and Bortolozzi, A. (2023). Sex-based modulation of endoplasmic reticulum stress and antidepressant response in a mouse model of α -synucleinopathy. *Neurosci. Applied* 2, 101028. <https://doi.org/10.1016/j.nsa.2023.101028>.
 89. Timberlake II, M., Roy, B., and Dwivedi, Y. (2019). A Novel Animal Model for Studying Depression Featuring the Induction of the Unfolded Protein Response in Hippocampus. *Mol. Neurobiol.* 56, 8524–8536. <https://doi.org/10.1007/s12035-019-01687-6>.
 90. Li Timberlake, M., and Dwivedi, Y. (2019). Linking unfolded protein response to inflammation and depression: potential pathologic and therapeutic implications. *Mol. Psychiatry* 24, 987–994. <https://doi.org/10.1038/s41380-018-0241-z>.
 91. Sidrauski, C., McGeachy, A.M., Ingolia, N.T., and Walter, P. (2015). The small molecule ISRIB reverses the effects of eIF2 α phosphorylation on translation and stress granule assembly. *Elife* 4, e05033. <https://doi.org/10.7554/eLife.05033>.
 92. Krystal, J.H., Kavalali, E.T., and Monteggia, L.M. (2024). Ketamine and rapid antidepressant action: new treatments and novel synaptic signaling mechanisms. *Neuropsychopharmacology* 49, 41–50. <https://doi.org/10.1038/s41386-023-01629-w>.
 93. Gartside, S.E., Cole, A.J., Williams, A.P., McQuade, R., and Judge, S.J. (2007). AMPA and NMDA receptor regulation of firing activity in 5-HT neurons of the dorsal and median raphe nuclei. *Eur. J. Neurosci.* 25, 3001–3008. <https://doi.org/10.1111/j.1460-9568.2007.05577.x>.
 94. Franklin, K.B.J., and Paxinos, G. (2008). *The Mouse Brain in Stereotaxic Coordinates* (Elsevier Academic Press).
 95. Halliday, M., Radford, H., Sekine, Y., Moreno, J., Verity, N., le Quesne, J., Ortori, C.A., Barrett, D.A., Fromont, C., Fischer, P.M., et al. (2015). Partial restoration of protein synthesis rates by the small molecule ISRIB prevents neurodegeneration without pancreatic toxicity. *Cell Death Dis.* 6, e1672. <https://doi.org/10.1038/cddis.2015.49>.
 96. Gao, C., Chen, X., Xu, H., Guo, H., Zheng, L., Yan, Y., Ren, Z., Luo, C., Gao, Y., Wang, Z., et al. (2022). Restraint Stress Delays the Recovery of Neurological Impairments and Exacerbates Brain Damages through Activating Endoplasmic Reticulum Stress-mediated Neurodegeneration/Autophagy/Apoptosis post Moderate Traumatic Brain Injury. *Mol. Neurobiol.* 59, 1560–1576. <https://doi.org/10.1007/s12035-022-02735-4>.
 97. Alarcón-Arís, D., Pavia-Collado, R., Miquel-Rio, L., Coppola-Segovia, V., Ferrés-Coy, A., Ruiz-Bronchal, E., Galofré, M., Paz, V., Campa, L., Revilla, R., et al. (2020). Anti- α -synuclein ASO delivered to monoamine neurons prevents α -synuclein accumulation in a Parkinson's disease-like mouse model and in monkeys. *EBioMedicine* 59, 102944. <https://doi.org/10.1016/j.ebiom.2020.102944>.

STAR★METHODS

KEY RESOURCES TABLE

REAGENT or RESOURCE	SOURCE	IDENTIFIER
Antibodies		
Rabbit anti-GABA	Sigma-Aldrich	Cat#A2052; RRID:AB_477652
Sheep anti-TPH	Sigma-Aldrich	Cat#AB1541; RRID:AB_90754
Rabbit anti-Iba1	FUJIFILM Wako	Cat#016-20001; RRID:AB_839506
Mouse anti-beta-Actin-Peroxidase (AC-15)	Sigma-Aldrich	Cat#A3854; RRID:AB_262011
Rabbit anti-BiP (C50B12)	Cell Signaling Technology	Cat#3177; RRID:AB_2119845
Mouse anti-CHOP (9C8)	ThermoFisher Scientific	Cat#MA1-250; RRID:AB_2292611
Rabbit anti-eEF2	Cell Signaling Technology	Cat#2332; RRID:AB_10693546
Rabbit anti-p-eEF2	Cell Signaling Technology	Cat#2331; RRID:AB_10015204
Rabbit anti-eIF2 α	Cell Signaling Technology	Cat#9722; RRID:AB_2230924
Rabbit anti-p-eIF2 α	Cell Signaling Technology	Cat#9721; RRID:AB_330951
Rabbit anti-GRP94	Abcam	Cat#ab3674; RRID:AB_303992
Rabbit anti-BDNF	Abcam	Cat#ab108319; RRID:AB_10862052
Rabbit anti-NeuN	Abcam	Cat#ab177487; RRID:AB_2532109
Rabbit anti-GFAP	Agilent Dako	Cat#Z0334; AB_10013382
HRP Rabbit α -mouse IgG	Abcam	Cat#ab6728; RRID:AB_955440
HRP Goat Anti-Rabbit IgG	Abcam	Cat#ab205718; RRID:AB_2819160
Biotin Rabbit Anti-Sheep IgG	Vector Labs	Cat#BA-6000; RRID:AB_2336217
Biotin Goat Anti-Rabbit IgG	Vector Labs	Cat#BA-1000; RRID: AB_2313606
Chemicals, peptides, and recombinant proteins		
LPS from <i>Escherichia coli</i> O127:B8	Sigma-Aldrich	Cat#L3129
Corticosterone	Sigma-Aldrich	Cat#C2505; CAS Number: 50-22-6
Dimethylsulfoxide	Sigma-Aldrich	Cat#34869; CAS Number: 67-68-5
PRONASE® Protease, <i>Streptomyces griseus</i>	Merck Millipore	Cat#53702; CAS Number: 9036-06-0
[33P]-dATP (>2500 Ci/mmol)	DuPont-NEN	N/A
Terminal deoxynucleotidyl-transferase	Roche	Cat#3333566001
Ilford K5 nuclear emulsion	Harman Technology Limited	Cat#10581
Kodak D-19 developer	Sigma-Aldrich	Cat#74200
Ilford Hypam fixer	Sigma-Aldrich	Cat#1758285
3,3'-Diaminobenzidine tetrahydrochloride	Sigma-Aldrich	Cat#D5905; CAS Number: 7411-49-6
Protease inhibitor: cOmplete™ ULTRA Tablets, Mini, EASYpack Protease Inhibitor Cocktail	Sigma-Aldrich	Cat#5892970001
Phosphatase inhibitor: PhosSTOP™	Sigma-Aldrich	Cat#4906837001
Pierce™ BCA Protein Assay Kit	Thermo Fisher Scientific	Cat#23227
SuperSignal Chemiluminescence ECL substrate kit	Thermo Fisher Scientific	Cat#34580
Entellan® Rapid Mounting Media for Microscope Slides	Electron Microscopy Sciences	Cat#14800
5-HT hydrochloride	Sigma-Aldrich	Cat#H9523; CAS Number: 153-98-0
(±)-8-OH-DPAT hydrobromide	Sigma-Aldrich	Cat#H8520; CAS Number: 87394-87-4
Citalopram hydrobromide	Tocris Bioscience	Cat#1427; CAS Number: 59729-32-7
Veratridine	Tocris Bioscience	Cat#2918; CAS Number: 71-62-5
Tunicamycin from <i>Streptomyces</i> sp.	Sigma-Aldrich	Cat#T7765; CAS Number: 11089-65-9

(Continued on next page)

Continued

REAGENT or RESOURCE	SOURCE	IDENTIFIER
<i>trans</i> -ISRIB	Tocris Bioscience	Cat#5284; CAS Number: 1597403-47-8
Salubrial	Santa Cruz Biotechnology	Cat#sc-202332; CAS Number: 405060-95-9

Experimental models: Organisms/strains

Mouse: C57BL6/J (male, 8 weeks)	Charles River	Cat#632
Mouse: NMRI (male, 8 weeks)	Envigo	Cat#275

Oligonucleotides

Egr-1 probe: 5'- GCATCATCTCCTCCAGTTTGGG GTAGTTGTCCATGGTGGGTGAGT -3'	Microsynth	NM_007913.5
BDNF probe: 5'- ACCCATGGGATTACACTTGGT CTCGTAGAAATACTGCTTCAGTTGGCCTT -3'	IDA Nucleic Acids Synthesis	NM_007540
TrkB probe: 5'- CGTGCAGATGGCAGACCACAA TTGGGTATCTGCAGTTGCCAGGGGCAT -3'	IDA Nucleic Acids Synthesis	NM_001025074
Neuritin probe: 5'- CACATATCTTTGCCCCCTT CCTGGCAATCCGTAAGAGCTG -3'	IBA Nucleic Acids Synthesis	NM_153529
PSD95 probe: 5'- GGCCTGCACCAGGTAAGCT ATTTGCACCGCGAGGATCAGT -3'	IDA Nucleic Acids Synthesis	NM_007864
VEGF probe: 5'- GTGCCCCCGTCCCTGGCC TTGCTTGCTCCCCGCGAGGCAAAGGACTTC -3'	IDA Nucleic Acids Synthesis	NM_001025250
GluN1 probe: 5'- GGGCGAATGTCAGCAGGTG CATGGTGCTCATGAGCTCCGGGCACA -3'	IDA Nucleic Acids Synthesis	N/A
GluN2B probe: 5'- AAGTGCCACGAGGATGA CAGCGATGCCGATGCTGGGGGGGCTCT -3'	IDA Nucleic Acids Synthesis	NM_008171
GluN2D probe: 5'- TGGCGCACGCCAGCGCCAG CAGCAGCAGCATCTTAGCGGGGCCCC -3'	IDA Nucleic Acids Synthesis	NM_008172

Software and algorithms

Fiji / ImageJ v1.53c	NIH	https://imagej.nih.gov/ij/
Prism v9.5.1	GraphPad	https://www.graphpad.com/
ImageLab software	https://www.bio-rad.com/es-es/product/image-lab-software?ID=KRE6P5E8Z	Version 6.1.0

Other

Carestream® BioMax® MR film	Sigma-Aldrich	Cat#Z350370
4–15% Mini-PROTEAN® TGX™ Precast Protein Gels, 15-well, 15 µl	Bio-rad	Cat#4561086
Trans-Blot Turbo Mini 0.2 µm Nitrocellulose Transfer Packs	Bio-rad	Cat#1704158

RESOURCE AVAILABILITY

Lead contact

Further information and requests for resources and reagents should be directed to and will be fulfilled by the Lead Contact, Analia Bortolozzi (analia.bortolozzi@iibb.csic.es).

Materials availability

This study did not generate new unique reagents.

Data and code availability

- All data reported in this paper will be shared by the [lead contact](#) upon request.
- This study does not report any original code.
- Any additional information required to reanalyze the data reported in this paper is available from the [lead contact](#) upon request.

EXPERIMENTAL MODEL AND STUDY PARTICIPANT DETAILS

Animals

Adult C57BL/6J mice (8 weeks; n=295, Charles River, Lyon, France) were used to generate the corticosterone (CORT, male mice) and tunicamycin-induced ERS (Tm, male and female mice) models. In addition, male NMRI mice (8 weeks; n=18, Envigo, Indiana, USA) were used in the lipopolysaccharide (LPS) model. All animals were housed in groups of five under controlled conditions ($22 \pm 1^\circ\text{C}$; 12h light/dark cycle) with food and water available *ad-libitum*. All experiments were performed with age-matched controls and different sets of animals were used for each experiment. Animal procedures were designed according to the 3R's rules and conducted in accordance with standard ethical guidelines (EU directive 2010/63 of 22 September 2010) and approved by the local Bioethics Committee (200/20, University of Barcelona).

LPS mouse model

LPS from *Escherichia coli* O127:B8 (Sigma-Aldrich, Madrid, Spain) was dissolved in saline and administered at a dose of 0.83 mg/kg, i.p. (10 ml/kg) at 8:00 pm.⁴¹ Behavioral evaluation was conducted 12 h following LPS administration. 30 min after the end of the behavioral assessment, mice were euthanized by cervical dislocation and brain samples were processed for Western blot (WB) analysis.

CORT mouse model

Mice were randomly distributed in control and CORT group before the treatment, and animal weight balance was equally represented in both groups. CORT (Sigma-Aldrich) was dissolved in commercial mineral water and adjusted to a pH 7.0-7.4 with HCl. Decreasing CORT concentrations were presented to mice for 28 days: 30 $\mu\text{g/ml}$ during 15 days (resulting in a dose of approximately 6.6 mg/kg/day), followed by 15 $\mu\text{g/ml}$ (2.7 mg/kg/day) during 3 days, and 7.5 $\mu\text{g/ml}$ (1.1 mg/kg/day) during 10 days; for a gradual recovery of endogenous corticosterone plasma.⁴⁰ CORT solution was available *ad libitum* in drinking water (opaque bottles) and was renewed every 72 hours. To verify CORT consumption, bottles' weight was checked each time the solution was renewed. Control mice followed the same experimental approach without CORT in their bottles. Mice from both groups were subjected to behavioral evaluation at day 36, and then were euthanized by cervical dislocation and brain samples were processed for WB analysis.

Tunicamycin mouse model

A stock solution of tunicamycin (Tm, 5 mg/ml, Sigma-Aldrich) was prepared in dimethyl sulfoxide (DMSO, Sigma-Aldrich). Isoflurane-anesthetized mice of both sexes (doses: 4% induction, 2% maintenance) were randomly injected with 1 μl of: i) Tm 200 $\eta\text{g}/\mu\text{l}$ (1:25 dilution from the stock solution), or ii) vehicle (4% DMSO in aCSF: NaCl, 125mM; KCl, 2.5mM; CaCl_2 , 1.26mM and MgCl_2 , 1.18mM) into dorsal raphe nuclei-DR (anterior-posterior AP: -4.5; medial-lateral ML: -1.0; dorsal-ventral DV: -3.2 in mm, relative to Bregma with an angle 20°)⁹⁴ using an electronic pump (Harvard Apparatus, Holliston, MA, USA) at a flow rate of 0.25 $\mu\text{l}/\text{min}$. An additional control group of mice received intra-DR 1 μl of aCSF under the same conditions. After infusion, the needle was kept in the injection site for additional 2 min to avoid reflux. The dose of Tm was chosen based on previous studies reporting acute activation of ERS and UPR signaling in the midbrain dopaminergic system.⁴⁶ In different cohorts of mice, behavioral assessments and histological or WB analyses were performed at 1, 3 and 7 days after Tm infusion.

METHOD DETAILS

Groups and drug treatments

In Experiment 1, 24 h after local infusion of vehicle or Tm, mice were randomly divided into four groups to explore whether ketamine recovers Tm-induced ERS in 5-HT neurons in DR: 1) Vehicle + Vehicle, 2) Tm + Vehicle, 3) Vehicle + Ketamine, and 4) Tm + Ketamine. Mice in groups 3 and 4 were intraperitoneally injected with a single dose of ketamine (10 mg/kg, ip, Ketolar®, Pfizer, Madrid, Spain), as previously reported.^{12,62} Groups 1 and 2 were treated with saline solution. Mice in the different groups were subjected to the different behavioral tests 30 min or 48 h later (corresponding to the 1-day and 3-day Tm groups, respectively), and then euthanized by cervical dislocation and brain was rapidly removed for WB or histological analyses.

In Experiment 2, various studies were performed to investigate the possible molecular mechanisms by which ketamine acts on PERK-eIF2 α signaling in DR. Mice receiving intra-DR infusion of vehicle or Tm were randomly divided into the following groups: 1) Vehicle + Vehicle + Vehicle, 2) Tm + Vehicle + Vehicle, 3) Tm + Vehicle + Ketamine, 4) Tm + ISRIB + Ketamine, and 5) Tm + Salubrinal + Ketamine. Mice in groups 4 and 5 received two doses of ISRIB (0.25 mg/kg, ip, Tocris Madrid, Spain) or salubrinal (1 mg/kg, ip, Santa Cruz Biotechnology, Dallas, TX, USA), one together with Tm and one 24 h later. Stock solutions of ISRIB or salubrinal (2 mg/ml) were prepared in DMSO (administered at 1:25 dilution from the stock solution). The dosing regimen with ISRIB or SAL was chosen as reported in the literature.^{95,96} Mice in groups 1, 2, and 3 were treated with DMSO 4% in NaCl 0.9% under the same conditions. Ketamine was administered in a single dose of 10 mg/kg (ip) and 30 min later behavioral effects were evaluated. At the end of the experiment, the animals were euthanized and their brains were removed for further analyses.

In Experiment 3, we investigated whether PERK-eIF2 α signaling is a potential target of antidepressant action under ERS in DR. Mice receiving intra-DR infusion of vehicle or Tm were randomly divided into the following groups: 1) Vehicle + Vehicle, 2) Vehicle + ISRIB, 3) Vehicle + Salubrinal, 4) Tm + Vehicle, 5) Tm + ISRIB, and 6) Tm + Salubrinal. ISRIB and Salubrinal were administered similarly to Experiment 2, and behavioral outcome was assessed 30 min after last administration. At the end of the experiment, mice were euthanized and their brains were removed for further WB or histological analyses.

Behavioral analysis

Different behavioral paradigms were used to evaluate anxiety and depressive-like phenotype. All tests were performed between 10:00 and 16:00 h by an experimenter blind to mouse treatments. On the day of testing, mice were moved to a dimly lit behavioral room and left undisturbed for at least 1 h prior to testing. Mice were tested in random order and the equipment was thoroughly cleaned with ethanol 75% between each trial to minimize odors.

Open field test (OFT)

Motor activity was measured in a plexiglas open field box (35 × 35 × 40 cm) indirectly illuminated (25–40 lux) to avoid reflection and shadows. The box floor was covered with an interchangeable opaque plastic base that was replaced for each animal. Motor activity was recorded during 15 min by a camera connected to a computer (Video-track, Viewpoint). The following variables were measured: horizontal locomotor and exploratory activity, defined as the total distance moved in cm, as well as the mean speed during the trial (cm/s).

Light and dark box test (DLB)

The apparatus consisted of two glass boxes (27 × 21 cm) with an interconnecting grey plastic tunnel (7 × 10 cm). One of these boxes was painted in black, being weakly lit by a red 25-W bulb (42 lux). The other box was lit by a 60-W desk lamp (400 lux) placed 30 cm above the box, which provided the unique laboratory illumination. At the beginning of the test, mice were placed individually in the middle of the dark area facing away from the opening, and were videotaped during 5 min. The following parameters were recorded: 1) number of entries to the lit box and 2) latency of the initial movement from the dark to the lit box. A mouse was considered to enter the new zone when more than half of its body was in the zone. The floor of each box was cleaned between mice.

Tail suspension test (TST)

Mice were suspended 30 cm above the bench by adhesive tape placed approximately 1 cm from the tip of the tail. Sessions were videotaped for 6 min and the immobility time was measured (Smart, Panlab, Cornella, Spain).

In situ hybridization (ISH)

Mice were euthanized by cervical dislocation and brains were rapidly removed, frozen on dry ice and stored at -80°C . Coronal tissue sections containing prefrontal cortex (PFC), cingulate cortex (Cg), caudate-putamen (CPu), hippocampus (HPC), amygdala (Amg), habenular nuclei (Hb), and dorsal raphe nucleus (DR) (14 μm -thick) were obtained and processed, as described elsewhere.^{12,40,62} Antisense oligoprobes were complementary to bases: GluN1 (GenBank accession NM_008169), GluN2B (NM_008171), GluN2D (NM_008172), BDNF (NM_007540), TrkB (NM_001025074), Neurtin (NM_153529), PSD95 (NM_007864), VEGF (NM_001025250), and Egr1 (NM_007913.5). Frozen tissue sections were fixed for 20 min at 4°C in 4% paraformaldehyde in phosphate-buffered saline (1x PBS: 8 mM Na_2HPO_4 , 1.4 mM KH_2PO_4 , 136 mM NaCl, and 2.6 mM KCl), washed for 5 min in 3xPBS at room temperature, twice for 5 min each in 1x PBS, and incubated for 2 min at 21°C in a solution of predigested pronase (Merck Millipore, Madrid, Spain) at a final concentration of 24 U/mL in 50 mM Tris-HCl, pH 7.5, and 5 mM EDTA. The enzymatic activity was stopped by immersion for 30 s in 2 mg/ml glycine in 1x PBS. Tissues were finally rinsed in 1xPBS and dehydrated through a graded series of ethanol.

Oligonucleotides were individually labeled (2 pmol) at the 3'-end with [^{33}P]-dATP (>2500 Ci/mmol; DuPont-NEN, Boston, MA, USA) using terminal deoxynucleotidyl-transferase (TdT, Calbiochem, La Jolla, CA, USA). For hybridization, the radioactively labelled probes were diluted in a solution containing 50% formamide, 4x standard saline citrate, 1x Denhardt's solution, 10% dextran sulfate, 1% sarkosyl, 20 mM phosphate buffer, pH 7.0, 250 $\mu\text{g}/\text{ml}$ yeast tRNA, and 500 $\mu\text{g}/\text{ml}$ salmon sperm DNA. The final concentration of radioactive probes in the hybridization buffer was in the range (~ 1.5 nM). Tissue sections were covered with hybridization solution containing the labelled probes, overlaid with parafilm coverslips and incubated overnight at 42°C in humid boxes. Sections were then washed 4 times (45 min each) in a buffer containing 0.6 M NaCl and 10 mM Tris-HCl (pH 7.5) at 60°C . Hybridized sections were exposed to Biomax-MR film (Sigma-Aldrich) for 1-4 weeks at -70°C with intensifying screens. For specificity control, adjacent sections were incubated with an excess (50x) of unlabeled probes. Films were analyzed and relative optical densities were evaluated in three adjacent sections by duplicate of each mouse, and averaged to obtain individual values using ImageJ (v1.53c, NIH, Bethesda, MD, USA) software. Contrast and brightness of images were the only variables digitally adjusted.

In addition, midbrain sections hybridized with Egr1, GluN1, GluN2B or GluN2D (NMDAR subunits) were then immersed in Ilford K5 nuclear emulsion (Harman Technology Limited) diluted 1:1 with distilled water. They were exposed in the dark conditions at 4°C for 1 week, and finally developed in Kodak D19 (Sigma-Aldrich) for 5 min, and fixed in Ilford Hypam fixer (Harman Technology Limited). Subsequently, tryptophan hydroxylase - TPH (anti-TPH; 1:2000; ref: AB1541, Sigma-Aldrich) staining was performed on both dipped Egr1 or NMDA subunit hybridized slides, while GABA (anti-GABA; 1:500; ref: A2052, Sigma-Aldrich) staining was performed on dipped Egr1 hybridized slides only. Briefly, following endogenous peroxidase inhibition, pre-incubation and incubation were carried out in a 1x PBS/Triton 0.2% solution containing normal serum from secondary antibody host. Primary antibody was incubated 2 days at 4°C , followed by incubation with the corresponding biotinylated secondary antibody. The color reaction was performed by incubation with diaminobenzidine tetrahydrochloride solution (DAB, Sigma-Aldrich). Sections were mounted and embedded in Entellan (Electron Microscopy Sciences, Hatfield, PA, USA). Microphotographs from DR sections were acquired using a Nikon Eclipse E100 microscope (Nikon, Tokyo, Japan). The number of Egr1 mRNA labelling

TPH- and GABA-positive cells in DR were assessed in raphe sections corresponding to different antero-posterior levels -4.04 to -4.96 mm from bregma using ImageJ (v1.53c, NIH) software. All labelled cells within the counting frame were counted in three consecutive sections and three different microscope fields were analyzed in each section.

Western Blot (WB)

The procedure for Western blot was as previously described.⁹⁷ Midbrain samples containing DR were dissected out using a Mouse Brain Matrix (Ted Pella, Madrid, Spain) and homogenized in RIPA buffer (150 mM NaCl, 50 mM Tris, pH 8.0, 1% Triton X-100, 0.5% Sodium deoxycholate, 5 mM EDTA, 0.1% SDS) with protease and phosphatase inhibitors. Proteins were quantified using Pierce™ BCA Protein Assay Kit (ThermoFisher Scientific, Waltham, MA, USA). Protein lysate (10 µg) was separated using 4–15% SDS-PAGE (Bio-Rad, Hercules, CA, USA) and electro-transferred onto a nitrocellulose membrane (Bio-Rad). Protein blots were incubated overnight at 4°C with primary antibodies: anti-BiP (1:1000; ref.: #3177, Cell Signaling Technologies, Danvers, MA, USA), anti-GRP94 (1:1000; ref.: ab3674, Abcam), anti-CHOP (1:500; ref.: #MA1-250, ThermoFisher Scientific), anti-p-eEF2 (1:500; ref.: #2331, Cell Signaling Technologies), anti-eEF2 (1:1000; ref.: #2332, Cell Signaling Technologies), anti-p-eIF2α (1:500; ref.: #9721, Cell Signaling Technologies), anti-eIF2α (1:1000; ref.: #9722, Cell Signaling Technologies), anti-BDNF (1:1000; ref.: ab108319, Abcam), anti-NeuN (1:1000; ref.: ab177487, Abcam), anti-Iba1 (1:1000; ref.: 016-20001, FUJIFILM Wako, Osaka, Japan), anti-GFAP (1:2500; ref.: Z0334, Agilent Dako, Santa Clara, CA, USA), and anti-β-Actin–Peroxidase (1:50000; ref.: A3854, Sigma-Aldrich) as loading control.

Detection was done by chemiluminescence using SuperSignal Chemiluminescence ECL substrate kit (Thermo Fisher Scientific), and pictures were taken using ChemiDoc Imaging System (Bio-Rad). Images were analyzed using ImageLab software (Bio-Rad).

In vivo microdialysis

All reagents used were of analytical grade and were obtained from Merck (Darmstadt, Germany). 5-HT hydrochloride and 8-OH-DPAT hydrobromide were obtained from Sigma-Aldrich, while veratridine was purchased from Tocris. To assess local effects in microdialysis experiments, veratridine was dissolved in aCSF and administered by reverse dialysis at the stated concentrations (uncorrected for membrane recovery). Veratridine stock solution was prepared in DMSO and diluted to appropriate concentrations in aCSF to reach 1% DMSO. 8-OH-DPAT was dissolved in saline solution and prepared daily. Extracellular 5-HT concentration was measured by *in vivo* microdialysis as previously described.⁵⁶ Briefly, one concentric dialysis probe (Cuprophane membrane; 6000 Da molecular weight cut-off; 2.0 mm-long) was implanted in mPFC (AP: +2.2; ML: -0.2; DV: -3.4 in mm)⁹⁴ of isoflurane-anesthetized mice. Experiments were performed 24 h after surgery in freely moving mice. 5-HT levels in dialysate samples were determined using HPLC coupled to electrochemical detection (+0.7 V, Waters 2465, Cerdanyola, Spain), with 3-fmol detection limit. The mobile phase containing 0.15 M NaH₂PO₄·H₂O, 1.7 mM PICB8, 0.2 mM EDTA and 16 % methanol, adjusted to pH 2.8 with orthophosphoric acid, was pumped at 1 ml/min (Waters 515 HPLC pump). 5-HT was separated on a 2.6 µm particle size C18 column (7.5 x 0.46 cm, Kinetex, Phenomenex, Madrid, Spain) at 28°C.

QUANTIFICATION AND STATISTICAL ANALYSIS

All values are expressed as the mean ± standard error of the mean (SEM). Statistical comparisons were performed using appropriate statistical tests by GraphPad Prism 9.5.1 software, as indicated in each figure legend. Outlier values were identified by the Grubbs' test (i.e. Extreme Student zed Deviate, ESD, method) and excluded from the analysis when applicable. Differences among means were analyzed by either 1- or 2-way analysis of variance (ANOVA) or two-tailed t-test, as appropriate. When ANOVA showed significant differences, pairwise comparisons between means were subjected to Tukey's post-hoc test, Dunnett's or Sidak's multiple comparisons test as appropriate. Data was assumed to be normally distributed. Differences were considered significant when P < 0.05. Detailed statistical analysis contents are described in [supplemental information \(Files S1, S2, S3, S4, S5, S6, S7, S8, S9, S10, S11, S12, S13, and S14\)](#). Sample sizes were determined empirically based on our previous experiences and the review of similar experiments in literature. The numbers of animals used are described in the corresponding figure legends or on each graph.